Quantum Functionalities Via Feedback Amplification

Rion Shimazu◉ and Naoki Yamamoto*

Department of Applied Physics and Physico-Informatics, Keio University, Hiyoshi 3-14-1, Kohoku, Yokohama 223-8522, Japan

Feedback amplification is a key technique for synthesizing various functionalities, especially in electronic circuits involving op amps. This paper presents a quantum version of this methodology, where the general phase-preserving quantum amplifier and coherent (i.e., measurement-free) feedback are employed to construct various types of systems having useful functionalities: quantum versions of differentiator, integrator, self-oscillator, and active filters. The class of active filters includes the Butterworth filter, which can be used to enhance the capacity of an optical quantum communication channel, and the nonreciprocal amplifier, which enables measurement of a superconducting qubits system as well as protection of it by separating input from output fields. A particularly detailed investigation is performed on the active phase-canceling filter for realizing a broadband gravitational-wave detector; that is, the feedback-amplification method is used to construct an active filter that compensates the phase delay of the signal and eventually recovers the sensitivity in the high-frequency regime.

I. INTRODUCTION

The amplifier is an essential component in modern technological systems, and it is usually involved in those systems in some feedback form. Let us consider a classical amplification process $y = Gu$ where u and y are input and output signals, and $G > 1$ is the gain of the amplifier. Then by feeding a fraction of the output back to the input through the controller K, as depicted in Fig. 1, the input-output relation is modified to

$$y = G^{(\mathrm{FB})}u, \quad G^{(\mathrm{FB})} = \frac{G}{1 + GK} = \frac{1}{1/G + K}.$$

Then by making the gain G large, we find $y = (1/K)u$; hence if K is a passive device with gain $K < 1$, the entire system works as a robust amplifier, which is insensitive to the parameter change in G. The usefulness of this feedback-amplification technique [1,2] is not limited to realizing such a robust amplifier. That is, by combining high-gain amplifiers (op amps in the electrical circuits) with several passive devices such as resistors and capacitors, one can devise a variety of functional systems; e.g., integrator, active filters, switches, and self-oscillators [3].

This paper develops the quantum version of feedback-amplification theory, which is expected to be of particular relevance to make the existing quantum technological devices robust and further to engineer systems with functionalities. In fact this idea has been implicitly employed

in some specific systems [4,5]. An explicit research direction was addressed in Ref. [6], showing a general quantum analog to the above-described robust amplification method; more precisely, it is shown that a coherent (i.e., measurement-free) feedback control [7–14] of a high-gain phase-preserving amplifier [5,15–18] and a passive device (e.g., a beam splitter) yields a robust phase-preserving amplifier.

This paper begins with Sec. II to introduce the models of the quantum phase-preserving amplifier and some linear passive systems. Then, using those models, we extend the quantum feedback-amplification scheme presented in Ref. [6] from the Fourier domain to the Laplace domain (Sec. III), together with developing a basic stability test method (Sec. IV). We then apply the theory to construct systems having several useful functionalities: quantum versions of differentiator and integrator (Sec. V), self-oscillator (Sec. VI), and active filters (Sec. VII). As for the quantum integrator, it is proven applicable for improving the detection efficiency of an itinerant field. The ability to synthesize a quantum self-oscillator might also be useful for several purposes as in the classical case, such as analog quantum memory and frequency converter [19,20], though in this paper we do not provide a concrete example. Active filtering is a typical application of feedback amplification, which in our case includes the quantum version of the Butterworth filter [21] and nonreciprocal amplifier; the former is used to realize the steep roll-off characteristic in frequency, which enables the enhancement of the capacity of a quantum communication channel [22]; the latter
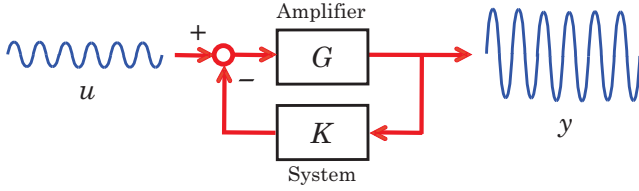
————
*yamamoto@appi.keio.ac.jp

FIG. 1.   Schematic of the classical feedback amplifier.

FIG. 2.   Nondegenerate parametric amplifier.

enables precise measurement of a superconducting qubits system while protecting it from the unwanted backward field generated in the amplification process [23–27].

In particular, in Sec. VIII we show a detailed investigation on the quantum phase-cancellation filter applied to the gravitational-wave detection problem; this is an active filter that can compensate the delayed phase of an incoming signal for the purpose of enhancing the detection bandwidth. The quantum phase-cancellation filters proposed in the literature [28–31] are based on an optomechanical implementation, but it requires an extremely low environmental temperature. The proposed phase-cancellation filter based on the feedback-amplification method, on the other hand, can be all-optically implemented at room temperature. We demonstrate a numerical simulation to show how much this filter can broaden the bandwidth of a typical gravitational-wave detector in a practical setting.

II. PRELIMINARIES

A. Phase-preserving linear amplifier

In this paper we consider a general phase-preserving linear amplifier [15,16,18]. A typical realization of this system is given by the *nondegenerate parametric amplifier (NDPA)* [5,32]. In the optics case, as depicted in Fig. 2, the NDPA is an optical cavity having two orthogonally polarized fields with modes a_1 and a_2, which are created and coupled with each other at the pumped nonlinear crystal (the green box in Fig. 2) inside the cavity. Also, the mode a_1 (a_2) couples with an input field b_1 (b_2) at the mirror with transmissibity proportional to γ. The Hamiltonian of the NDPA is given by

$$H_{\text{NDPA}} = \hbar\omega_1 a_1^\dagger a_1 + \hbar\omega_2 a_2^\dagger a_2$$
$$+ i\hbar\lambda(a_1^\dagger a_2^\dagger e^{-2i\omega_p t} - a_1 a_2 e^{2i\omega_p t}),$$

with ω_k the resonant frequencies of a_k, $\lambda \in \mathbb{R}$ the coupling strength between a_1 and a_2, and $2\omega_p$ the pump frequency. Here we assume that $\omega_1 = \omega_2 = \omega_p$. Then, in the rotating frame at frequency ω_p, the dynamics of the NDPA is given by the following Langevin equation [33]:

$$\begin{bmatrix} \dot{a}_1 \\ \dot{a}_2^\dagger \end{bmatrix} = \begin{bmatrix} -\gamma/2 & \lambda \\ \lambda & -\gamma/2 \end{bmatrix}\begin{bmatrix} a_1 \\ a_2^\dagger \end{bmatrix} - \sqrt{\gamma}\begin{bmatrix} b_1 \\ b_2^\dagger \end{bmatrix}. \quad (1)$$
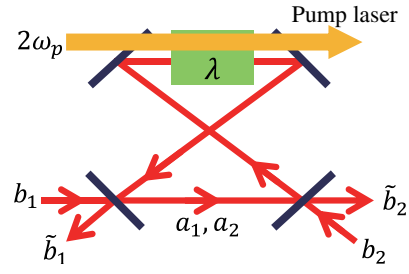
Note that the canonical commutation relation of input fields is given by $[b(t), b^\dagger(t')] = \delta(t - t')$, with $\delta(t - t')$ the Dirac δ function. The output equations are given by

$$\tilde{b}_1 = \sqrt{\gamma}a_1 + b_1, \quad \tilde{b}_2^\dagger = \sqrt{\gamma}a_2^\dagger + b_2^\dagger. \quad (2)$$

From Eqs. (1) and (2), the input-output relation of the NDPA is represented as

$$\begin{bmatrix} \tilde{b}_1(s) \\ \tilde{b}_2^\dagger(s^*) \end{bmatrix} = \frac{1}{(s + \gamma/2)^2 - \lambda^2}$$
$$\times \begin{bmatrix} s^2 - \lambda^2 - \gamma^2/4 & -\gamma\lambda \\ -\gamma\lambda & s^2 - \lambda^2 - \gamma^2/4 \end{bmatrix}$$
$$\times \begin{bmatrix} b_1(s) \\ b_2^\dagger(s^*) \end{bmatrix}. \quad (3)$$

The operator $b(s)$ is related to $b(t)$ via the Laplace transformation [6,34,35]:

$$b(s) = \int_0^\infty e^{-st}b(t)dt, \quad b^\dagger(s) = [b(s)]^\dagger$$
$$= \int_0^\infty e^{-s^*t}b^\dagger(t)dt.$$

From Eq. (3), $\gamma > 2\lambda$ if and only if the amplifier is stable [i.e., every solution of the characteristic polynomial $(s + \gamma/2)^2 - \lambda^2 = 0$ has a negative real part]. The output mode $\tilde{b}_1$ at $s = 0$ is given by

$$\tilde{b}_1(0) = -\frac{\gamma^2 + 4\lambda^2}{\gamma^2 - 4\lambda^2}b_1(0) + \frac{-4\gamma\lambda}{\gamma^2 - 4\lambda^2}b_2^\dagger(0),$$

which diverges as $\gamma \to 2\lambda + 0$. Hence, in this parameter limit, the signal with s satisfying $|s| \ll \gamma$ is largely amplified.

In this paper we consider the general phase-preserving linear amplifier with the following input-output relation:

$$\begin{bmatrix} \tilde{b}_1(s) \\ \tilde{b}_2^\dagger(s^*) \end{bmatrix} = G(s)\begin{bmatrix} b_1(s) \\ b_2^\dagger(s^*) \end{bmatrix},$$
$$G(s) = \begin{bmatrix} G_{11}(s) & G_{12}(s) \\ G_{21}(s) & G_{22}(s) \end{bmatrix}. \quad (4)$$

The condition on the transfer function matrix $G(s)$ is represented in the Fourier domain as follows. The Fourier transformation of the field operators are defined as

$$b(i\omega) = \int_{-\infty}^{\infty} e^{-i\omega t} b(t) dt,$$

$$b^\dagger(i\omega) = [b(i\omega)]^\dagger = \int_{-\infty}^{\infty} e^{i\omega t} b^\dagger(t) dt,$$

which satisfy $[b(i\omega), b^\dagger(i\omega')] = 2\pi\delta(\omega - \omega')$. This commutation relation requires $G(s)$ to satisfy

$$|G_{11}(i\omega)|^2 - |G_{12}(i\omega)|^2 = |G_{22}(i\omega)|^2 - |G_{21}(i\omega)|^2 = 1,$$

$$G_{21}(i\omega)G_{11}^*(i\omega) - G_{22}(i\omega)G_{12}^*(i\omega) = 0, \quad \forall\omega, \quad (5)$$

where $G_{ij}^*(i\omega) = [G_{ij}(i\omega)]^*$ is the complex conjugate of $G_{ij}(i\omega)$.

B. Passive systems

The general form of passive linear system from the inputs (b_3, b_4) to the outputs $(\tilde{b}_3, \tilde{b}_4)$ in the Laplace domain is represented as

$$\begin{bmatrix} \tilde{b}_3^\dagger(s^*) \\ \tilde{b}_4^\dagger(s^*) \end{bmatrix} = K(s) \begin{bmatrix} b_3^\dagger(s^*) \\ b_4^\dagger(s^*) \end{bmatrix},$$

$$K(s) = \begin{bmatrix} K_{11}(s) & K_{12}(s) \\ K_{21}(s) & K_{22}(s) \end{bmatrix}, \quad (6)$$

where the creation-mode representation is used to simplify the notation. The transfer function $K(s)$ satisfies $|K_{11}(i\omega)|^2 + |K_{12}(i\omega)|^2 = 1$, $|K_{21}(i\omega)|^2 + |K_{22}(i\omega)|^2 = 1$, and $K_{21}(i\omega)K_{11}^*(i\omega) + K_{22}(i\omega)K_{12}^*(i\omega) = 0$, $\forall\omega$. These conditions are derived from unitarity of the response function matrix of passive quantum system:

$$K^{-1}(i\omega) = K^\dagger(i\omega) = \begin{bmatrix} K_{11}^*(i\omega) & K_{21}^*(i\omega) \\ K_{12}^*(i\omega) & K_{22}^*(i\omega) \end{bmatrix}.$$

A typical passive device is a single-mode optical cavity having two input-output ports, depicted in Fig. 3(a). The dynamics of the cavity is given by

$$\dot{a}_3^\dagger = \left(-\frac{\kappa_1 + \kappa_2}{2} + i\Delta \right) a_3^\dagger - \sqrt{\kappa_1} b_3^\dagger - \sqrt{\kappa_2} b_4^\dagger,$$

where a_3 is the cavity mode, κ_i is the coupling strength between a_3 and the input itinerant field b_i, and Δ is the
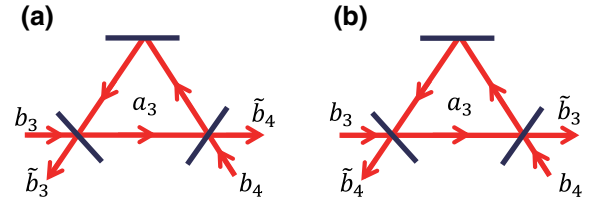

FIG. 3. Single-mode optical cavity, functioning as (a) the low-pass filter and (b) the high-pass filter, for the input-output relation from b_3 to $\tilde{b}_4$.

detuning. Also the output equations are given by

$$\tilde{b}_3^\dagger = \sqrt{\kappa_1} a_3^\dagger + b_3^\dagger, \quad \tilde{b}_4^\dagger = \sqrt{\kappa_2} a_3^\dagger + b_4^\dagger.$$

Then the transfer function matrix $K(s)$ is given by

$$K(s) = \frac{1}{s + (\kappa_1 + \kappa_2)/2 - i\Delta}$$
$$\times \begin{bmatrix} s + (\kappa_2 - \kappa_1)/2 - i\Delta & -\sqrt{\kappa_1\kappa_2} \\ -\sqrt{\kappa_1\kappa_2} & s + (\kappa_1 - \kappa_2)/2 - i\Delta \end{bmatrix}. \quad (7)$$

In the special case $\kappa_1 = \kappa_2 = \kappa$ and $\Delta = 0$, it is

$$K(s) = \frac{1}{s + \kappa} \begin{bmatrix} s & -\kappa \\ -\kappa & s \end{bmatrix}. \quad (8)$$

Hence the relation between b_3 and $\tilde{b}_4$ is given by

$$\tilde{b}_4^\dagger(s^*) = \frac{-\kappa}{s + \kappa} b_3^\dagger(s^*) + \frac{s}{s + \kappa} b_4^\dagger(s^*). \quad (9)$$

That is, in the domain $|s| \gg \kappa$, the cavity works as an integrator for the transmitting field from b_3 to $\tilde{b}_4$. Also it works as a low-pass filter with bandwidth κ; that is, the frequency components of b_3 with $|s| = |i\omega| \ll \kappa$ can only pass through the cavity, and hence this cavity is called the mode-cleaning cavity (MCC).

In this paper we also work on the case where $\tilde{b}_4$ is the reflected field of b_3, as shown in Fig. 3(b); in this case the transfer function is given by

$$K(s) = \frac{1}{s + (\kappa_1 + \kappa_2)/2 - i\Delta}$$
$$\times \begin{bmatrix} -\sqrt{\kappa_1\kappa_2} & s + (\kappa_1 - \kappa_2)/2 - i\Delta \\ s + (\kappa_2 - \kappa_1)/2 - i\Delta & -\sqrt{\kappa_1\kappa_2} \end{bmatrix}. \quad (10)$$

Again in the special case $\kappa_1 = \kappa_2 = \kappa$ and $\Delta = 0$, it is

$$K(s) = \frac{1}{s + \kappa} \begin{bmatrix} -\kappa & s \\ s & -\kappa \end{bmatrix}. \quad (11)$$

Hence the relation between b_3 and $\tilde{b}_4$ is given by

$$\tilde{b}_4^\dagger(s^*) = \frac{s}{s+\kappa} b_3^\dagger(s^*) + \frac{-\kappa}{s+\kappa} b_4^\dagger(s^*).$$

That is, at around $s = 0$, the cavity works as a differentiator for the reflected field from b_3 to $\tilde{b}_4$. Also it works as a high-pass filter with bandwidth κ; that is, the optical components of b_3 in the domain $|s| = |i\omega| \gg \kappa$ can only pass through the cavity. We also call this cavity a MCC.

III. QUANTUM FEEDBACK AMPLIFICATION

In this paper we consider the general feedback-connected system shown in Fig. 4, composed of the high-gain quantum phase-preserving amplifier G and a passive system K. The feedback structure is made by

$$\tilde{b}_2 = b_3, \quad b_2 = \tilde{b}_4,$$

which are of course the same as $\tilde{b}_2^\dagger = b_3^\dagger$ and $b_2^\dagger = \tilde{b}_4^\dagger$. The entire system has the inputs $(b_1, b_4^\dagger)$ and the outputs $(\tilde{b}_1, \tilde{b}_3^\dagger)$. From Eqs. (4) and (6), the input-output relation of this system is given by

$$\begin{bmatrix} \tilde{b}_1(s) \\ \tilde{b}_3^\dagger(s^*) \end{bmatrix} = G^{(\mathrm{FB})}(s) \begin{bmatrix} b_1(s) \\ b_4^\dagger(s^*) \end{bmatrix},$$

$$G^{(\mathrm{FB})}(s) = \begin{bmatrix} G_{11}^{(\mathrm{FB})}(s) & G_{12}^{(\mathrm{FB})}(s) \\ G_{21}^{(\mathrm{FB})}(s) & G_{22}^{(\mathrm{FB})}(s) \end{bmatrix}, \quad (12)$$

where

$$G_{11}^{(\mathrm{FB})} = \frac{G_{11} - K_{21}\det[G]}{1 - K_{21}G_{22}}, \quad (13)$$

$$G_{12}^{(\mathrm{FB})} = \frac{G_{12}K_{22}}{1 - K_{21}G_{22}}, \quad (14)$$

$$G_{21}^{(\mathrm{FB})} = \frac{G_{21}K_{11}}{1 - K_{21}G_{22}}, \quad (15)$$

$$G_{22}^{(\mathrm{FB})} = \frac{K_{12} + G_{22}\det[K]}{1 - K_{21}G_{22}}, \quad (16)$$

with $\det[G] = G_{11}G_{22} - G_{12}G_{21}$ and $\det[K] = K_{11}K_{22} - K_{12}K_{21}$. These matrix entries satisfy $|G_{11}^{(\mathrm{FB})}(i\omega)|^2 -$
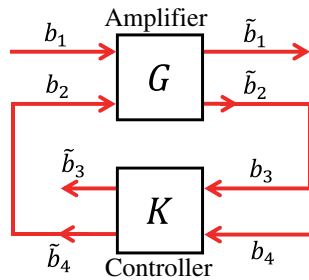

FIG. 4.   Feedback structure of the quantum amplifier.

$|G_{12}^{(\mathrm{FB})}(i\omega)|^2 = 1$, $\forall\omega$, etc., meaning that it also functions as a phase-preserving amplifier.

It was shown in Ref. [6] that $|G_{11}^{(\mathrm{FB})}(i\omega)| \approx 1/|K_{21}(i\omega)|$ holds in the high-gain amplification limit $|G_{11}(i\omega)| \to \infty$; because the characteristic change in the passive transfer function $K(s)$ is usually very small, this realizes the robust quantum amplification, which is the quantum analog to the classical feedback-amplification technique mentioned in the first paragraph in Sec. I. We now extend this idea to the Laplace domain. The point to derive the result is that, from Eq. (5), we have

$$\det[G(i\omega)] = G_{11}(i\omega)G_{22}(i\omega) - G_{12}(i\omega)\frac{G_{22}(i\omega)G_{12}^*(i\omega)}{G_{11}^*(i\omega)},$$

$$= \frac{[|G_{11}(i\omega)|^2 - |G_{12}(i\omega)|^2]G_{22}(i\omega)}{G_{11}^*(i\omega)}$$

$$= \frac{G_{22}(i\omega)}{G_{11}^*(i\omega)},$$

and thus

$$\frac{\det[G(i\omega)]}{G_{22}(i\omega)} = \frac{1}{G_{11}^*(i\omega)} \to 0,$$

in the high-gain limit $|G_{11}(i\omega)| \to \infty$. Also again from Eq. (5), $|G_{11}(i\omega)| = |G_{22}(i\omega)|$ and $|G_{12}(i\omega)| = |G_{21}(i\omega)|$ hold. Then in the same limit, Eq. (5) leads to

$$1 - \left|\frac{G_{12}(i\omega)}{G_{11}(i\omega)}\right|^2 = \frac{1}{|G_{11}(i\omega)|^2} \to 0$$

$$\implies \left|\frac{G_{12}(i\omega)}{G_{22}(i\omega)}\right| \to 1,$$

$$1 - \left|\frac{G_{21}(i\omega)}{G_{22}(i\omega)}\right|^2 = \frac{1}{|G_{22}(i\omega)|^2} \to 0$$

$$\implies \left|\frac{G_{21}(i\omega)}{G_{22}(i\omega)}\right| \to 1.$$

These are equivalent to

$$\frac{G_{12}(i\omega)}{G_{22}(i\omega)} \to e^{i\theta(\omega)}, \quad \frac{G_{21}(i\omega)}{G_{22}(i\omega)} \to e^{i\varphi(\omega)},$$

where $\theta(\omega)$ and $\varphi(\omega)$ are certain real functions of ω.

We now extend the above result and assume that

$$\frac{\det[G(s)]}{G_{22}(s)} \to 0, \quad \frac{G_{12}(s)}{G_{22}(s)} \to 1, \quad \frac{G_{21}(s)}{G_{22}(s)} \to 1 \quad (17)$$

hold in the domain $\mathcal{D} = \{s \in \mathbb{C} \,;\, |G_{11}(i\omega)| \to \infty\}$. Moreover, we assume $G_{11}(s) = G_{22}(s)$ for all $s \in \mathbb{C}$. These conditions are indeed satisfied in the case of NDPA shown in Sec. A, for s satisfying $|s| \ll \gamma$, where the high-gain limit is realized by taking $\gamma \to 2\lambda + 0$. Under the above

assumptions, the transfer function matrix of the entire closed-loop system can be approximated by

$$G^{(\text{FB})}(s) = \frac{-1}{K_{21}(s)} \begin{bmatrix} 1 & K_{22}(s) \\ K_{11}(s) & \det[K(s)] \end{bmatrix}, \quad (18)$$

in the domain $\mathcal{D}$. Hence, we now have a quantum system that, as proven later, generates several interesting and robust functionalities available in the feedback-amplification setting.

The proof of Eq. (18) is as follows:

$$G_{11}^{(\text{FB})} = \frac{G_{11} - K_{21}\det[G]}{1 - K_{21}G_{22}} = \frac{1 - K_{21}(\det[G]/G_{22})}{(1/G_{22}) - K_{21}}$$
$$\rightarrow -\frac{1}{K_{21}},$$

$$G_{12}^{(\text{FB})} = \frac{G_{12}K_{22}}{1 - K_{21}G_{22}} = \frac{(G_{12}/G_{22})K_{22}}{(1/G_{22}) - K_{21}} \rightarrow -\frac{K_{22}}{K_{21}},$$

$$G_{21}^{(\text{FB})} = \frac{G_{21}K_{11}}{1 - K_{21}G_{22}} = \frac{(G_{21}/G_{22})K_{11}}{(1/G_{22}) - K_{21}} \rightarrow -\frac{K_{11}}{K_{21}},$$

$$G_{22}^{(\text{FB})} = \frac{K_{12} + G_{22}\det[K]}{1 - K_{21}G_{22}} = \frac{(K_{12}/G_{22}) + \det[K]}{(1/G_{22}) - K_{21}}$$
$$\rightarrow -\frac{\det[K]}{K_{21}}.$$

We again emphasize that Eq. (18) is the system depending only on the passive component K, meaning that $G^{(\text{FB})}$ is robust against the characteristic change in G. Note that, for a general phase-preserving amplifier, which does not necessarily satisfy Eq. (17) and $G_{11}(s) = G_{22}(s) \ \forall s \in \mathbb{C}$, the resulting closed-loop system in the high-gain limit may still contain some components of G. Hence, following the convention of the classical feedback-amplification theory, we call G satisfying these assumptions the *ideal quantum op amp*.

IV. STABILITY ANALYSIS METHOD

From an engineering viewpoint, it is useful to guarantee the stability of the entire controlled system before activating it (more precisely, before closing the loop for control). In the classical case the seminal Nyquist method [36] is often used for this purpose. Here we show the quantum version of this method, particularly for the quantum feedback-controlled system with transfer function matrix. Eq. (12); note that, hence, the stability must be guaranteed for the system with finite amplification gain.

Let us represent the matrix entries of $G(s)$ and $K(s)$ as $G_{ij}(s) = g_{ij}(s)/g(s)$ and $K_{ij}(s) = k_{ij}(s)/k(s)$, respectively, where $g(s), g_{ij}(s), k(s)$, and $k_{ij}(s)$ are the polynomial functions. Then, it is easy to see that $G^{(\text{FB})}(s)$ has the following form:

$$G^{(\text{FB})}(s) = \frac{1}{g^2(s)k^2(s)\{1 - K_{21}(s)G_{22}(s)\}} \begin{bmatrix} \star & \star \\ \star & \star \end{bmatrix},$$

where for simplicity the matrix entries, the polynomial functions denoted by $\star$, are not shown. Here we assume that the original systems $G(s)$ and $K(s)$ are stable; then because $k(s)$ and $g(s)$ are stable polynomial functions [meaning that the zeros of $k(s)$ and $g(s)$ lie in the left side plane in $\mathbb{C}$], the stability of the closed-loop system is completely characterized by the zeros of $1 - K_{21}(s)G_{22}(s)$.

We can now apply the classical Nyquist method to test the stability of this closed-loop system. As in the classical case let us define the open-loop transfer function:

$$L(s) = -K_{21}(s)G_{22}(s).$$

Then, from the Nyquist theorem, the simplest stability criterion is as follows. If the point -1 lies outside the Nyquist plot [i.e., the trajectory of $L(i\omega)$ for $\omega \in (-\infty, +\infty)$ in the complex plane], then the closed-loop system is stable; otherwise, it is unstable. The point is that this stability test can be carried out for an open-loop system illustrated in Fig. 5, which is constructed via simply cascading the amplifier and the controller. In fact the input-output relation of this open-loop system is given by

$$\begin{bmatrix} \tilde{b}_1(s) \\ \tilde{b}_3^\dagger(s^*) \\ \tilde{b}_4^\dagger(s^*) \end{bmatrix} = G^{(\text{open})}(s) \begin{bmatrix} b_1(s) \\ b_2^\dagger(s^*) \\ b_4^\dagger(s^*) \end{bmatrix},$$

$$G^{(\text{open})}(s) = \begin{bmatrix} G_{11}(s) & G_{12}(s) & 0 \\ K_{11}(s)G_{21}(s) & K_{11}(s)G_{22}(s) & K_{12}(s) \\ K_{21}(s)G_{21}(s) & K_{21}(s)G_{22}(s) & K_{22}(s) \end{bmatrix}.$$

Therefore, the Nyquist plot can be obtained by setting b_1 and b_4 to the vacuum fields and injecting the coherent field $|\alpha e^{i\omega}\rangle$ in the b_2 port with several frequencies ω. In fact, measuring the amplitude of the output field $\tilde{b}_4$ gives us the Nyquist plot in the form $L(i\omega) = -\langle \tilde{b}_4^\dagger(-i\omega)\rangle/\alpha^*$. Note that the measurement result of $\tilde{b}_4$ must be probabilistic, and
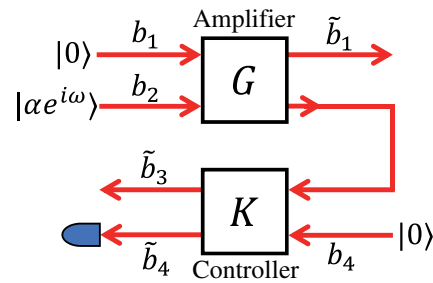

FIG. 5. System structure for the stability test of the closed-loop system.

hence the Nyquist plot constitutes a "band" with variance $\langle|\Delta\tilde{b}_4(i\omega)|^2\rangle$, meaning that the stability margin should be taken into account.

V. FUNCTIONALITIES 1: QUANTUM PROPORTIONAL INTEGRAL DIFFERENTIAL (PID)

We now start describing several functionalities realized by the developed quantum feedback-amplification method. The first functionality is the quantum PID [37]. That is, we show that, via the proper choice of the system K, the ideal closed-loop system, Eq. (18), functions as a differentiator (D) or integrator (I) on the input itinerant field b_1; hence together with the proportional component (P), which simply attenuates or amplifies the amplitude of the input, now P, I, and D components are provided to us. These three are clearly the most basic components involved in almost all electrical circuits and used for constructing several useful systems such as a PID feedback controller and an analog computer. In fact, a classical PID control for quantum systems has been proposed [38,39]; the fully quantum PID controller constructed using feedback amplification may have some advantages over the classical one, but we leave this analysis for future work. Instead, we show a simple application of the quantum integrator at the end of this section.

A. Differentiator

Let us take the symmetric cavity, Eq. (8), as the controller $K(s)$. In this case, the transfer function of the ideal closed-loop system, Eq. (18), is given by

$$G^{(\mathrm{FB})}(s) = \frac{1}{\kappa}\begin{bmatrix} s+\kappa & s \\ s & s-\kappa \end{bmatrix}.$$

Hence from Eq. (12), the output $\tilde{b}_3^\dagger(s)$ is given by

$$\tilde{b}_3^\dagger(s^*) = \frac{s}{\kappa}b_1(s) + \frac{s-\kappa}{\kappa}b_4^\dagger(s^*),$$

or in the time domain it is

$$\tilde{b}_3^\dagger(t) = \frac{1}{\kappa}\frac{d}{dt}b_1(t) + \frac{1}{\kappa}\frac{d}{dt}b_4^\dagger(t) - b_4^\dagger(t),$$

meaning that the closed-loop system works as a differentiator for the itinerant field $b_1(t)$.

As discussed in Sec. III, the approximation is valid only in a specific s region such that the high-gain limit is effective. To show a concrete example of this region, we study a feedback-controlled system composed of the optical NDPA and the control cavity, depicted in Fig. 6(a). Recall that, in the case of NDPA, the high-gain limit is achieved in the regime $|s| \ll \gamma \approx 2\lambda$, which becomes
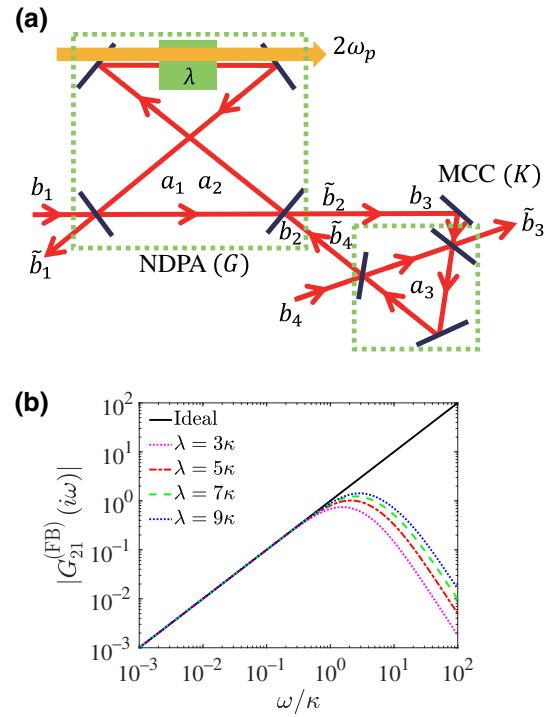

FIG. 6. (a) Optical realization of the quantum differentiator. (b) Gain plot of the actual transfer function, Eq. (15), and its ideal limit $|i\omega/\kappa|$ for the quantum differentiator.

wider as λ increases. Actually this can be seen in Fig. 6(b), showing the gain plot of the transfer function, Eq. (15), of this optical system with parameters $\gamma = 2.01\lambda$ and its high-gain limit $|i\omega/\kappa|$; that is, the frequency range such that this controlled system effectively approximates the ideal differentiator becomes wider as λ gets bigger.

Note that, as in the classical case, the differentiator itself is an unstable system, and thus this system should be used together with other components such that the entire system is stable. This instability can be readily seen using the method addressed in Sec. IV; the open-loop transfer function in this case is

$$L(s) = \frac{\kappa(s^2 - \gamma^2/4 - \lambda^2)}{(s+\kappa)(s^2 + \gamma s + \gamma^2/4 - \lambda^2)},$$

and the Nyquist plot is given by Figs. 7(a) and 7(b), showing that the point -1 lies inside the trajectory of $L(i\omega)$ and thus the system is unstable. Note that the actual Nyquist plot fluctuates along the curve shown in the figure, with variance $\langle|\Delta\tilde{b}_4(i\omega)|^2\rangle$.

B. Integrator

Next we take the high-pass filtering cavity, Eq. (11), as the controller, where in this case the reflected field is fed back to the amplifier, as shown in Fig. 8(a) in the optics case. Then the transfer function matrix, Eq. (18), of the
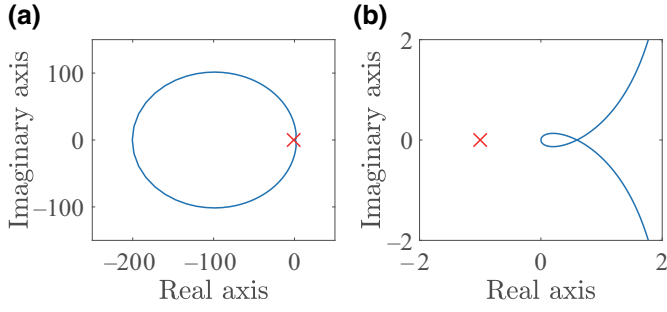
FIG. 7. (a) Nyquist plot of the quantum differentiator, where the parameters are set as $\kappa = 1$, $\lambda = 2\kappa$, and $\gamma = 2.01\lambda$. (b) Enlargement of (a) at around $s = 0$.

ideal closed-loop system is given by

$$G^{(\text{FB})}(s) = \frac{1}{s}\begin{bmatrix} -s - \kappa & \kappa \\ \kappa & s - \kappa \end{bmatrix}.$$

Hence from Eq. (12) the output $\tilde{b}_3^{\dagger}(s^*)$ is connected to the input $b_1(s)$ as

$$\tilde{b}_3^{\dagger}(s^*) = \frac{\kappa}{s} b_1(s) + \frac{s - \kappa}{s} b_4^{\dagger}(s^*),$$

or in the time domain it is

$$\tilde{b}_3^{\dagger}(t) = \kappa \int_0^t b_1(\tau)d\tau + b_4^{\dagger}(t) - \kappa \int_0^t b_4^{\dagger}(\tau)d\tau. \quad (19)$$

This means that in a specific s region where the high-gain limit of the amplifier is effective ($|s| \ll \gamma$ in the NDPA case, as discussed in Sec. III), the closed-loop system works as an integrator for the itinerant field $b_1(t)$. Note again that the feedback-controlled system can approximate the integrator in the low-frequency regime, while the standard noncontrolled cavity, Eq. (9), can do the same task in a high-frequency regime $|i\omega| \gg \kappa$; in this sense the integrator shown here is the functionality realized only via the feedback-amplification method.

Now, unlike the differentiator, the integrator forms a circulating field in the feedback loop between the amplifier and the controller cavity. Therefore, we regard this loop as another cavity with mode a_4, as depicted in Fig. 8(b) in the optics case and Fig. 8(c) in a microwave system case, which we call the loop cavity. In fact, for the model depicted in Fig. 8(a) where b_2, $\tilde{b}_2$, b_3, and $\tilde{b}_4$ are treated as the itinerant fields, they violate the Ito rule such as $dB_2(t)dB_2^{\dagger}(t) = dt$ with $B_2(t) = \int_0^t b_2(\tau)d\tau$ [33,40]. In what follows we show that this modified model still maintains the functionality of integration. More precisely, we
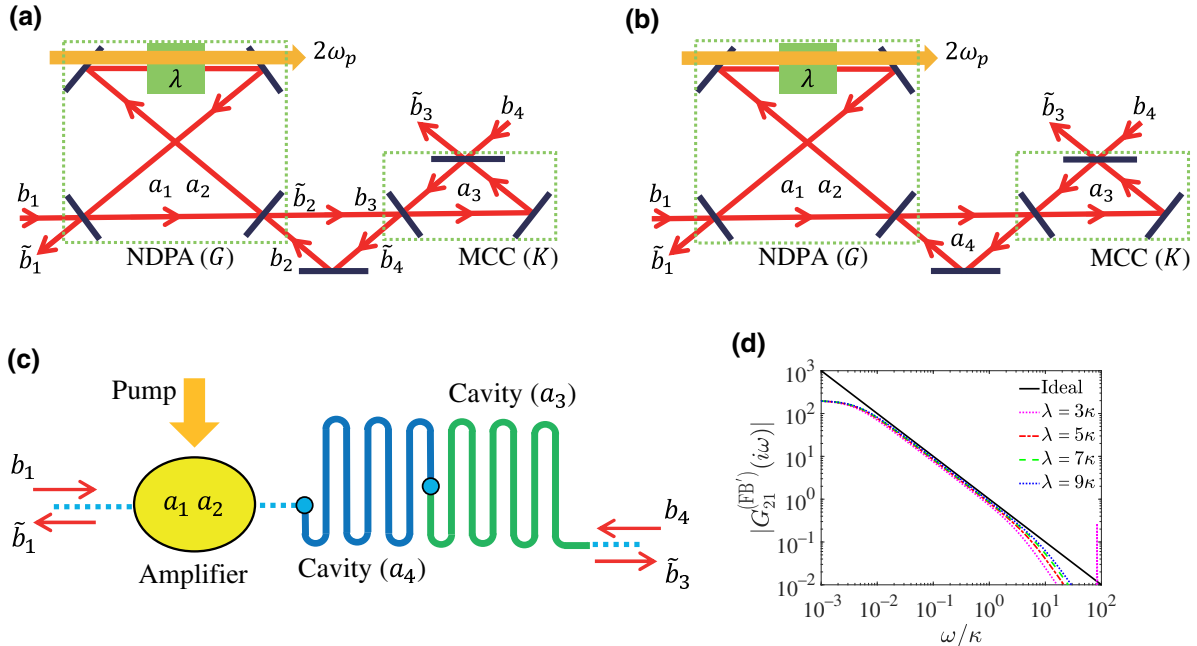
FIG. 8.   (a) Optical realization of the quantum integrator with input b_1 and output $\tilde{b}_3$. (b) Modified model for the quantum integrator where the loop between the NDPA and MCC is regarded as a cavity with the mode a_4. (c) Microwave realization of the quantum integrator. (d) Gain plot of the actual transfer function $|G_{21}^{(\text{FB}')}(i\omega)|$ in Eq. (23) and its ideal limit $|\kappa/i\omega|$. The spike around $\omega/\kappa \approx 10^2$ is due to invalid approximation in the high-frequency region.

show that the transfer function from b_1 to $\tilde{b}_3^\dagger$ in Fig. 8(b) or Fig. 8(c) approaches to κ/s in the same high-gain limit.

First, the Hamiltonian of the system is given by

$$H_{\text{FB amp}} = \sum_{k=1}^{4} \hbar\omega_k a_k^\dagger a_k + i\hbar\lambda(a_1^\dagger a_2^\dagger e^{-2i\omega_p t} - a_1 a_2 e^{2i\omega_p t})$$
$$+ \hbar g_{24}(a_2^\dagger a_4 + a_2 a_4^\dagger) + \hbar g_{34}(a_3^\dagger a_4 + a_3 a_4^\dagger),$$
$$(20)$$

where ω_3 and ω_4 are the resonant frequencies of a_3 and a_4, respectively. g_{24} (g_{34}) describes the coupling strength between a_2 and a_4 (a_3 and a_4), which are given by

$$g_{24} = \sqrt{c\gamma/L_4}, \quad g_{34} = \sqrt{c\kappa/L_4}, \quad (21)$$

with L_4 the round-trip length of the loop cavity and $c = 3 \times 10^8$ m/s the speed of light. Here we assume $\omega_k = \omega_p$ ($k = 1, \ldots, 4$). Together with the coupling to the external fields, we find that, in the rotating frame at frequency ω_p, the dynamical equations are given by

$$\dot{a}_1 = -\frac{\gamma}{2}a_1 + \lambda a_2^\dagger - \sqrt{\gamma}b_1, \quad \dot{a}_2^\dagger = \lambda a_1 + ig_{24}a_4^\dagger,$$

$$\dot{a}_3^\dagger = -\frac{\kappa}{2}a_3^\dagger + ig_{34}a_4^\dagger - \sqrt{\kappa}b_4^\dagger, \quad \dot{a}_4^\dagger = ig_{24}a_2^\dagger + ig_{34}a_3^\dagger,$$

$$\tilde{b}_1 = \sqrt{\gamma}a_1 + b_1, \quad \tilde{b}_3^\dagger = \sqrt{\kappa}a_3^\dagger + b_4^\dagger.$$
$$(22)$$

The input-output equation of this system in the Laplace domain is of the form

$$\begin{bmatrix} \tilde{b}_1(s) \\ \tilde{b}_3^\dagger(s^*) \end{bmatrix} = \begin{bmatrix} G_{11}^{(\text{FB'})}(s) & G_{12}^{(\text{FB'})}(s) \\ G_{21}^{(\text{FB'})}(s) & G_{22}^{(\text{FB'})}(s) \end{bmatrix} \begin{bmatrix} b_1(s) \\ b_4^\dagger(s^*) \end{bmatrix},$$

where particularly $G_{21}^{(\text{FB'})}(s)$ is given by

$$G_{21}^{(\text{FB'})}(s) = \frac{\alpha_0}{s^4 + \beta_3 s^3 + \beta_2 s^2 + \beta_1 s + \beta_0}, \quad (23)$$

with

$$\alpha_0 = \sqrt{\gamma\kappa}\lambda g_{24}g_{34}, \quad \beta_0 = \gamma\kappa g_{24}^2/4 - \lambda^2 g_{34}^2,$$
$$\beta_1 = (\gamma g_{24}^2 + \kappa g_{24}^2 + \gamma g_{34}^2 - \kappa\lambda^2)/2,$$
$$\beta_2 = \gamma\kappa/4 - \lambda^2 + g_{24}^2 + g_{34}^2, \quad \beta_3 = (\gamma + \kappa)/2.$$

In the limit $\gamma \to 2\lambda + 0$, together with Eq. (21), the above coefficients are approximated as

$$\alpha_0 \approx 2c\kappa\lambda^2/L_4, \quad \beta_0 \approx 0,$$
$$\beta_1 \approx 2c\lambda(\kappa + \lambda)/L_4 - \kappa\lambda^2/2,$$
$$\beta_2 \approx \kappa\lambda/2 - \lambda^2 + c(\kappa + 2\lambda)/L_4, \quad \beta_3 \approx \kappa/2 + \lambda.$$

Furthermore, we assume $|s| \ll \gamma$, so that the higher-order term of s can be neglected. Then the transfer function,

Eq. (23), can be approximated by

$$G_{21}^{(\text{FB'})}(s) \approx \frac{\alpha_0}{\beta_1 s} \approx \frac{2c\kappa\lambda^2/L_4}{\{2c\lambda(\kappa + \lambda)/L_4 - \kappa\lambda^2/2\}s}$$
$$= \frac{\kappa}{\left(1 + \dfrac{\kappa}{\lambda} - \dfrac{L_4\kappa}{4c}\right)s}.$$

Thus, if $\kappa \ll \lambda$ and $L_4\kappa/(4c) \ll 1$, this system becomes the integrator, which we wish to obtain:

$$G_{21}^{(\text{FB'})}(s) \approx \frac{\kappa}{s}.$$

In Fig. 8(d), the solid black line shows the ideal gain plot of the integrator, (i.e., $|\kappa/i\omega|$), while the dotted lines represent $|G_{21}^{(\text{FB'})}(i\omega)|$ in Eq. (23) with parameters $\gamma = 2.01\lambda$, $c/L_4 = 10^3\kappa$, and $\lambda = n\kappa$ ($n = 3, 5, 7, 9$). Clearly, $|G_{21}^{(\text{FB'})}(i\omega)|$ well approximates $|\kappa/i\omega|$ in a specific s region where the high-gain limit of the NDPA is effective, which is now given by $|s| \ll \gamma \approx 2\lambda$. Hence, λ should be relatively large to guarantee that the integrator works in a wider region in s; this can be actually seen in the figure, although making λ large does not make a big difference in the parameter regime considered here. However, the approximation is not valid in the frequency domain where $\omega/\kappa < 10^{-2}$. This is because, if $s = 0$, the transfer function in Eq. (23) is $G_{21}^{(\text{FB'})}(0) = \alpha_0/\beta_0$, whereas the transfer function of the integrator goes towards infinity if $s \to 0$. Therefore, the approximation is valid in the relatively low-frequency domain where s^4, s^3, s^2 can be ignored and where $|\beta_1 s| \gg |\beta_0| (\Leftrightarrow |s| \gg |\beta_0/\beta_1|)$.

The stability of the modified model depicted in Figs. 8(b) and 8(c) cannot be investigated via the stability test discussed in Sec. IV, which can only be applied to the case where the feedback loop does not form a cavity. Therefore, instead of Nyquist's theorem, we use the *Routh-Hurwitz method* [41]. In our case, the system is stable if and only if every root of the characteristic polynomial function in the denominator in Eq. (23) has a negative real part; the Routh-Hurwirz method systematically leads to the stability condition as follows:

$$\beta_3 > 0, \quad \frac{\beta_2\beta_3 - \beta_1}{\beta_3} > 0, \quad \frac{\beta_3^2\beta_0}{\beta_1 - \beta_2\beta_3} + \beta_1 > 0.$$

Note that $\beta_3 > 0$ is already satisfied.

C. Application to qubit detection

Here we give an application of the integrator, which can be used in a stand-alone fashion unlike the differentiator. The system of interest (not the feedback-controlled system) is a qubit that is dissipatively coupled to the external itinerant field $b_0(t)$, such as a transmon qubit coupled to

a superconducting resonator; the Langevin equation of the system variable $\sigma_x(t)$ is given by

$$\frac{d}{dt}\sigma_x(t) = -\frac{\Gamma}{2}\sigma_x(t) + \sqrt{\Gamma}\sigma_z(t)\{b_0(t) + b_0^\dagger(t)\},$$

where Γ is the strength of the dissipative coupling [33]. The output field is given by $b_1(t) = \sqrt{\Gamma}\sigma_-(t) + b_0(t)$; the quadrature $q_1(t) = \{b_1(t) + b_1^\dagger(t)\}/\sqrt{2}$ thus follows

$$q_1(t) = \sqrt{\frac{\Gamma}{2}}\sigma_x(t) + \frac{b_0(t) + b_0^\dagger(t)}{\sqrt{2}}.$$

Now the field state is set to the vacuum $|0\rangle_F$. Then we find

$${}_F\langle 0|q_1(t)|0\rangle_F = \sqrt{\frac{\Gamma}{2}}e^{-\Gamma t/2}\sigma_x,$$

where for a system-field operator X, ${}_F\langle 0|X|0\rangle_F$ represents an operator living in the system Hilbert space. This means that, for a very short time interval $\Gamma t \ll 1$, the above operator is approximated as ${}_F\langle 0|q_1(t)|0\rangle_F \approx \sqrt{\Gamma/2}\sigma_x$, which thus takes $\pm\sqrt{\Gamma/2}$ when measuring it. In other words, to measure the qubit state we need a high-speed detector.

Using the integrator changes this condition. Let us place the ideal integrator having the input-output relation, Eq. (19), along the output field of the qubit. That is, the output $b_1(t)$ is taken as the input to the integrator, and we measure its output $\tilde{b}_3(t)$. The quadrature $\tilde{q}_3(t) = \{\tilde{b}_3(t) + \tilde{b}_3^\dagger(t)\}/\sqrt{2}$ then satisfies

$$\begin{aligned} {}_F\langle 0|\tilde{q}_3(t)|0\rangle_F &= {}_F\langle 0|\left(\kappa\int_0^t \frac{b_1(\tau) + b_1^\dagger(\tau)}{\sqrt{2}}d\tau\right)|0\rangle_F \\ &= \kappa\sqrt{\frac{2}{\Gamma}}(1 - e^{-\Gamma t/2})\sigma_x, \end{aligned}$$

where b_4 is set to be a vacuum field. Therefore, in the long time limit $\Gamma t \gg 1$, this output itinerant field becomes

$${}_F\langle 0|\tilde{q}_3(t)|0\rangle_F \approx \kappa\sqrt{\frac{2}{\Gamma}}\sigma_x.$$

Hence the measurement result is $\pm\kappa\sqrt{2/\Gamma}$, which equal is to $\pm\sqrt{\Gamma/2}$ by choosing the integrator parameter as $\kappa = \Gamma/2$. This means that, even if the given detector is slow, the integrator assists it to capture the same amount of measurement signal as that obtained by a fast detector.

VI. FUNCTIONALITIES 2: SELF-OSCILLATION

Self-oscillation is also an useful functionality realized with the feedback-amplification method, which is indeed widely used in a variety of engineering scenes. To realize a sustained oscillation, of course, some nonlinearities

such as a voltage saturation are necessary to be involved, but here we focus only on the linear part; a possible practical application of the proposed method, which combines a nonlinear component will be presented in a future work.

Let us consider the cavity, Eq. (10), with $\kappa_1 = \kappa_2 = \kappa$. Then the transfer function of the ideal closed-loop system, Eq. (18), is given by

$$G^{(\mathrm{FB})}(s) = \frac{1}{s - i\Delta}\begin{bmatrix} s + \kappa - i\Delta & -\kappa \\ \kappa & s - \kappa - i\Delta \end{bmatrix}.$$

Therefore, the output $\tilde{b}_3$ is given by

$$\tilde{b}_3^\dagger(s^*) = \frac{\kappa}{s - i\Delta}b_1(s) + \frac{s - \kappa - i\Delta}{s - i\Delta}b_4^\dagger(s^*).$$

Because the pole is on the imaginary axis, this represents a self-oscillation of $\tilde{b}_3$. In fact, if both b_1 and b_4 are set to the vacuum and $\langle\tilde{b}_3(0)\rangle \neq 0$, then in the time domain $\tilde{b}_3$ satisfies

$$\langle\tilde{b}_3(t)\rangle = e^{-i\Delta t}\langle\tilde{b}_3(0)\rangle, \tag{24}$$

hence it oscillates with frequency $-\Delta$ (in the rotating frame). Also, the spectral broadening of this oscillation can be seen from

$$\frac{1}{2\pi}\int_{-\infty}^{\infty}\langle\tilde{b}_3^\dagger(-i\omega)\tilde{b}_3(-i\omega')\rangle d\omega' = \frac{\kappa^2}{(\omega - \Delta)^2}.$$

In practice, the cavity parameter $\kappa_1 - \kappa_2$ is set to a small positive number, which makes the system oscillating almost with a fixed frequency yet with growing amplitude; but the amplitude is saturated by some dissipative nonlinearities, and as a result a sustained oscillation called the quantum limit cycle can be realized. As in the classical case, there may be several applications of this functionality, e.g., a quantum memory [19] and synchronization for spectroscopy [42]; also see Ref. [43] for the general semiclassical method for analyzing the quantum limit cycle and synchronization.

Now we show the dynamics of the entire closed-loop system in nearly the ideal amplification limit. In the optics case, the realization of the self-oscillator is very similar to the integrator shown in Fig. 8(a). The only difference between the self-oscillator and the integrator is that the detuning of the MCC is not zero for the case of the self-oscillator, while it is zero for the integrator. Also as in the integrator, the self-oscillator forms a loop cavity between the NDPA and MCC, and thus it should be modeled as the system shown in Fig. 8(b) or Fig. 8(c) with nonzero detuning Δ in the mode a_3. Then the entire dynamical equation of the self-oscillator is the same as those in Eqs. (22) except that $i\Delta a_3^\dagger$ is added to the right-hand side of the

equation that has a term $\dot{a}_3^\dagger$ in the left-hand side. Here, if $\langle b_1(t)\rangle = \langle b_4^\dagger(t)\rangle = 0 \; \forall t$, the mean dynamics is

$$\frac{d}{dt}\begin{bmatrix}\langle a_1\rangle \\ \langle a_2^\dagger\rangle \\ \langle a_3^\dagger\rangle \\ \langle a_4^\dagger\rangle\end{bmatrix} = A_{\mathrm{osc}}\begin{bmatrix}\langle a_1\rangle \\ \langle a_2^\dagger\rangle \\ \langle a_3^\dagger\rangle \\ \langle a_4^\dagger\rangle\end{bmatrix}, \quad \langle \tilde{b}_3^\dagger\rangle = \sqrt{\kappa}\,\langle a_3^\dagger\rangle,$$

where

$$A_{\mathrm{osc}} = \begin{bmatrix}-\gamma/2 & \lambda & 0 & 0 \\ \lambda & 0 & 0 & ig_{24} \\ 0 & 0 & -\kappa/2+i\Delta & ig_{34} \\ 0 & ig_{24} & ig_{34} & 0\end{bmatrix}.$$

Figure 9 shows the mean time evolution of the quadratures of $\tilde{b}_3(t)$:

$$\tilde{q}_3(t) = \frac{\tilde{b}_3(t)+\tilde{b}_3^\dagger(t)}{\sqrt{2}}, \quad \tilde{p}_3(t) = \frac{\tilde{b}_3(t)-\tilde{b}_3^\dagger(t)}{\sqrt{2}i}.$$

The parameters and the initial conditions are set as follows: $\Delta = 1$, $\lambda = 0.01\Delta$, $\gamma = 2.01\lambda$, and $c/L_4 = 0.1\Delta$. Also κ is set to $\kappa = 0.1\Delta$ (black lines in the figure) or $\kappa = 0.01\Delta$ (light blue lines). The initial condition is $\langle a_1(0)\rangle = \langle a_2^\dagger(0)\rangle = \langle a_3^\dagger(0)\rangle = \langle a_4^\dagger(0)\rangle = 1/\sqrt{2}$. Now the ideal oscillation, Eq. (24), is represented in terms of the quadratures as

$$\begin{bmatrix}\langle\tilde{q}_3(t)\rangle \\ \langle\tilde{p}_3(t)\rangle\end{bmatrix} = \begin{bmatrix}\cos(\Delta t) & \sin(\Delta t) \\ -\sin(\Delta t) & \cos(\Delta t)\end{bmatrix}\begin{bmatrix}\langle\tilde{q}_3(0)\rangle \\ \langle\tilde{p}_3(0)\rangle\end{bmatrix}.$$

With the initial values mentioned above, these are given by $\langle\tilde{q}_3(t)\rangle = \sqrt{\kappa}\cos(\Delta t)$ and $\langle\tilde{p}_3(t)\rangle = -\sqrt{\kappa}\sin(\Delta t)$, meaning that there is a $\pi/2$ phase difference between the two quadratures. Figure 9 shows that the case $\kappa = 0.01\Delta$ closely reproduces this ideal oscillation. In particular, the
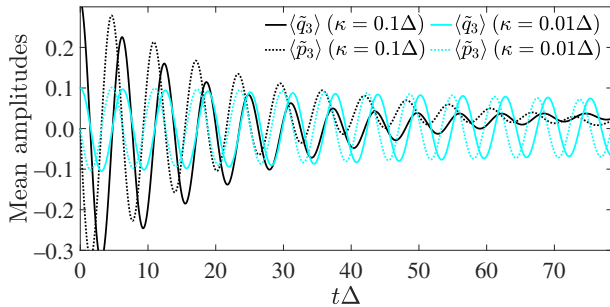

FIG. 9.   Time evolution of the quadratures of $\tilde{b}_3$. Note that the amplitudes will eventually diverge due to instability of the self-oscillator, which is not illustrated in the figure; in practice, such divergence is suppressed via some nonlinearity.

smaller value of κ leads to the slower attenuation of the oscillation. This is simply because the smaller κ is, the fewer photons leak out from the MCC with detuning Δ. Thus, by setting κ smaller, we can preserve the coherence of the light field oscillating with frequency Δ in the MCC. However, making κ smaller also reduces the amount of photons coming from the NDPA into the MCC, and thus the amplitude of oscillation is limited. Conversely, a large value of κ allows a large amount of photons to flow from NDPA to MCC, resulting in a large oscillation amplitude, as demonstrated in the case $\kappa = 0.1\Delta$ in Fig. 9. Therefore, there is a trade-off between the coherence time and the amplitude of the self-oscillation.

VII. FUNCTIONALITIES 3: ACTIVE FILTERS

As we see in Sec. B, the two-input two-output cavity works as a low-pass or high-pass filter with bandwidth κ and maximal gain 1. Here we show that, by the feedback-amplification method, several types of filter with tunable bandwidth, gain, and phase, i.e., the quantum version of active filters, can be engineered.

A. High-Q active filter

First we show a simple first-order active filter. As in the quantum integrator, the controller is chosen as the high-pass filtering cavity, Eq. (10), with zero detuning $\Delta = 0$, which in this case is set to be asymmetric (i.e., $\kappa_1 \neq \kappa_2$). Then, the closed-loop , Eq. (18), realized in the high-gain amplification limit is given by

$$\begin{bmatrix}\tilde{b}_1(s) \\ \tilde{b}_3^\dagger(s^*)\end{bmatrix} = G^{(\mathrm{FB})}(s)\begin{bmatrix}b_1(s) \\ b_4^\dagger(s^*)\end{bmatrix},$$

$$G^{(\mathrm{FB})}(s) = \frac{1}{s+(\kappa_2-\kappa_1)/2}$$
$$\times \begin{bmatrix}-s-(\kappa_1+\kappa_2)/2 & \sqrt{\kappa_1\kappa_2} \\ \sqrt{\kappa_1\kappa_2} & s-(\kappa_1+\kappa_2)/2\end{bmatrix}. \tag{25}$$

Here we focus on the output $\tilde{b}_3^\dagger(s^*)$:

$$\tilde{b}_3^\dagger(s^*) = \frac{\sqrt{\kappa_1\kappa_2}}{s+(\kappa_2-\kappa_1)/2}b_1(s) + \frac{s-(\kappa_1+\kappa_2)/2}{s+(\kappa_2-\kappa_1)/2}b_4^\dagger(s^*),$$

with $\kappa_2 - \kappa_1 > 0$. Hence, this system functions as a low-pass filter for $b_1(s)$ with bandwidth $(\kappa_2-\kappa_1)/2$. In contrast to the standard low-pass filter, Eq. (8), with bandwidth κ, the bandwidth of this active filter can be made very small by making κ_1 and κ_2 close to each other. As a result, the Q factor can be largely enhanced from $Q = \omega_0/2\kappa$ to $Q' = \omega_0/(\kappa_2-\kappa_1)$. For instance, for a coherent light field with frequency $\omega_0 = 3\times 10^{14}$ Hz, an optical cavity $\kappa = 3\times 10^6$ leads to $Q = 5\times 10^7$, while the active filter with

$\kappa_1 = \kappa$ and $\kappa_2 = 1.01\kappa$ leads to $Q' = 1 \times 10^{10}$. Note that this active filter also functions as an amplifier with gain $2\sqrt{\kappa_1\kappa_2}/(\kappa_2 - \kappa_1)$, which becomes large if the Q factor increases. It is noteworthy that, in this case, the idler noise mode b_4 is also amplified with gain $(\kappa_2 + \kappa_1)/(\kappa_2 - \kappa_1)$ at $s = 0$. This means that basically the filtering makes sense only for an input field with amplitude much bigger than $(\kappa_2 + \kappa_1)/(\kappa_2 - \kappa_1)$. Also we remark that, as discussed in the case of the integrator, the feedback loop now constructs another cavity, which should be taken into account for more precise modeling of the filter; we give such a detailed investigation in Sec. VIII for another type of active filter discussed in the next subsection.

B. Phase-cancellation filter

The functionality provided by an active filter is not only modifying the gain profile, but changing the phase of an input field. In fact Miao *et al.* proposed a quantum active filter that can effectively change the phase and thereby enhance the bandwidth of the gravitational-wave detector or, in a wider sense, any cavity-based quantum sensor [28]. A rough description of their idea is as follows. When a gravitational wave propagates through the interferometer (arm cavity), then it must pick up a phase $\phi_{\mathrm{arm}}(\Omega) = -2\Omega L_{\mathrm{arm}}/c$, where Ω, L_{arm}, and c are the gravitational-wave frequency, the length of the cavity, and c the speed of light, respectively. Note that only in Secs. B and VIII we use the conventional Ω rather than ω to recall that this is the gravitational-wave frequency. This extra phase eventually limits the bandwidth of the detector; hence constructing an auxiliary intracavity filter with the transfer function $e^{-i\phi_{\mathrm{arm}}(\Omega)} = e^{2i\Omega L_{\mathrm{arm}}/c}$ will compensate this extra phase and thus may recover the bandwidth.

Here we show that the feedback-amplification method can be employed to realize such a phase-canceling filter in a fully optical setting. We again use the closed-loop system, Eq. (25), and now consider the output $\tilde{b}_1$:

$$\tilde{b}_1(s) = G_{11}^{(\mathrm{FB})}(s)b_1(s) + G_{12}^{(\mathrm{FB})}(s)b_4^\dagger(s^*)$$
$$= -\frac{s + (\kappa_1 + \kappa_2)/2}{s + (\kappa_2 - \kappa_1)/2}b_1(s) + \frac{\sqrt{\kappa_1\kappa_2}}{s + (\kappa_2 - \kappa_1)/2}b_4^\dagger(s^*).$$

Let us then set $\kappa_2 = 0$:

$$\tilde{b}_1(s) = G_{11}^{(\mathrm{FB})}(s)b_1(s) = -\frac{s + \kappa_1/2}{s - \kappa_1/2}b_1(s). \qquad (26)$$

In the frequency domain $s = i\Omega$ this equation reduces to

$$\tilde{b}_1(i\Omega) = G_{11}^{(\mathrm{FB})}(i\Omega)b_1(i\Omega) = -\frac{i\Omega + \kappa_1/2}{i\Omega - \kappa_1/2}b_1(i\Omega).$$

Then by setting $\Omega \ll \kappa_1$ and $\kappa_1 = 2c/L_{\mathrm{arm}}$, we actually find that $G_{11}^{(\mathrm{FB})}$ approximates our target filter:

$$G_{11}^{(\mathrm{FB})}(i\Omega) = \frac{-\Omega^2 + \kappa_1^2/4 + i\Omega\kappa_1}{\Omega^2 + \kappa_1^2/4} \approx \frac{\kappa_1^2/4 + i\Omega\kappa_1}{\kappa_1^2/4},$$
$$\approx e^{4i\Omega/\kappa_1} = e^{2i\Omega L_{\mathrm{arm}}/c} = e^{-i\phi_{\mathrm{arm}}(\Omega)}. \qquad (27)$$

This phase-canceling filter might be realizable in practice by carefully devising the controller cavity so that the optical loss κ_2 is very small. Note that in the literature works [28–31] an optomechanical oscillator was employed to realize the same filter where in that case κ_2 represents the magnitude of the thermal bath added on the oscillator; hence $\kappa_2 \approx 0$ requires the oscillator to be in an ultralow temperature environment.

Lastly note that the system, Eq. (26), is clearly unstable; particularly the system, Eq. (27), represents a phase-lead filter that violates the causality. Similar to the case of the integrator, therefore, in a practical setting such a phase-cancellation filter must be incorporated in a bigger system that is totally stable. In Sec. VIII we give a detailed study to see how much the phase-cancellation filter, Eq. (26), could compensate the phase delay and thereby enhance the bandwidth of the stabilized gravitational-wave detector in a practical setup.

C. Butterworth filter

Let us move back to the problem of modifying the gain profile via an active filter. A particularly useful bandpass filter, which is often used in classical electrical circuits, is the Butterworth filter. The transfer function of the nth-order classical Butterworth filter is given by $T_n(s) = g/B_n(s)$ where g is a constant and the following are examples of polynomials $B_n(s)$:

$$B_1(s) = s + 1, \quad B_2(s) = s^2 + \sqrt{2}s + 1,$$
$$B_3(s) = (s + 1)(s^2 + s + 1).$$

The gain of the filter is given by

$$|T_n(i\omega)| = \frac{g}{\sqrt{(\omega/\omega_B)^{2n} + 1}},$$

which has the steep roll-off characteristic of frequency, particularly for large n, at the cutoff frequency ω_B.

A quantum version of Butterworth filter has actually been employed in the literature; in Ref. [22], a fourth-order quantum Butterworth filter was applied to enhance the channel capacity of a linear time-invariant bosonic channel. However, its physical realization has not been discussed. Here we show that, in the simple case $n = 2$, the feedback-amplification technique can be used to realize the quantum Butterworth filter.
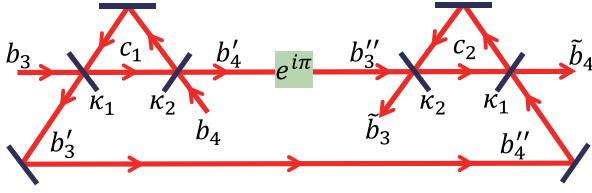
FIG. 10. The controller K for realizing the second-order quantum Butterworth filter in the optical setting. The detuning of the left cavity is Δ, while that of the right cavity is $-\Delta$. This controller has the inputs (b_3, b_4) and outputs $(\tilde{b}_3, \tilde{b}_4)$. A phase shifter is embedded between the two cavities.

The controller K is chosen as the cascaded cavities, an optical case of which is depicted in Fig. 10. The left cavity with mode c_1 has two inputs (b_3, b_4) and two outputs (b_3', b_4'), and the right one with mode c_2 has two inputs (b_3'', b_4'') and two outputs $(\tilde{b}_3, \tilde{b}_4)$. We assume that the detuning of the left and right cavities are Δ and $-\Delta$, respectively. A phase shifter $e^{i\pi} (= -1)$ is placed in the path from b_4' to b_3''. Then the two input and output fields are connected as follows:

$$b_3''^\dagger(s^*) = -b_4'^\dagger(s^*), \quad b_4''^\dagger(s^*) = b_3'^\dagger(s^*).$$

The input-output relations of each cavities are given by

$$\begin{bmatrix} b_3'^\dagger(s^*) \\ b_4'^\dagger(s^*) \end{bmatrix} = K_l(s) \begin{bmatrix} b_3^\dagger(s^*) \\ b_4^\dagger(s^*) \end{bmatrix},$$

$$\begin{bmatrix} \tilde{b}_3^\dagger(s^*) \\ \tilde{b}_4^\dagger(s^*) \end{bmatrix} = K_r(s) \begin{bmatrix} b_3''^\dagger(s^*) \\ b_4''^\dagger(s^*) \end{bmatrix},$$

where $K_l(s)$ is given by the left-hand side of Eq. (7) and

$$K_r(s) = \frac{1}{s + (\kappa_1 + \kappa_2)/2 + i\Delta}$$
$$\times \begin{bmatrix} s + (\kappa_1 - \kappa_2)/2 + i\Delta & -\sqrt{\kappa_1 \kappa_2} \\ -\sqrt{\kappa_1 \kappa_2} & s - (\kappa_1 - \kappa_2)/2 + i\Delta \end{bmatrix}.$$

The transfer function of the controller is thus given by

$$K(s) = K_r(s) \begin{bmatrix} 0 & -1 \\ 1 & 0 \end{bmatrix} K_l(s). \tag{28}$$

Here we set $\Delta = (\kappa_1 + \kappa_2)/2$. The feedback configuration is depicted in Fig. 4, where $K(s)$ is now given by Eq. (28). Then from Eqs. (18) and (28), we find that the output $\tilde{b}_3^\dagger$ of the closed-loop system composed of this controller and a
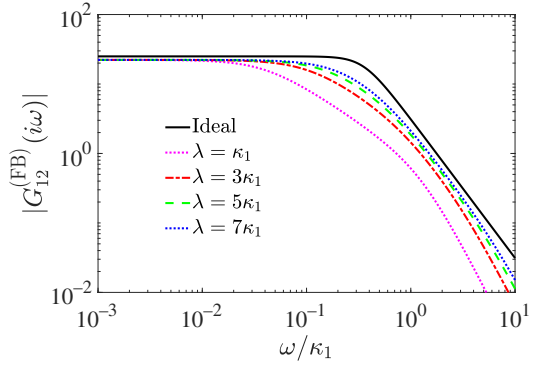

FIG. 11. Gain plot of the ideal second-order quantum Butterworth filter (black solid line) and that of actual transfer function $G_{21}^{(FB)} = G_{21} K_{11}/(1 - K_{21} G_{22})$ with several λ (dotted lines).

high-gain amplifier G is given by

$$\tilde{b}_3^\dagger(s) = G_{21}^{(FB)}(s) b_1(s) + G_{22}^{(FB)}(s) b_4^\dagger(s^*),$$
$$= -\frac{\{\kappa_1 - \kappa_2 + i(\kappa_1 + \kappa_2)\} \sqrt{\kappa_1 \kappa_2}}{s^2 + (\kappa_2 - \kappa_1)s + (\kappa_2 - \kappa_1)^2/2} b_1(s)$$
$$-\frac{s^2 - (\kappa_2 + \kappa_1)s + (\kappa_2 + \kappa_1)^2/2}{s^2 + (\kappa_2 - \kappa_1)s + (\kappa_2 - \kappa_1)^2/2} b_4^\dagger(s^*).$$

The transfer function from b_1 to $\tilde{b}_3^\dagger$ has a form of the second-order Butterworth filter with cutoff frequency $\omega_B = (\kappa_2 - \kappa_1)/\sqrt{2}$ and maximal gain $g = \sqrt{2\kappa_1 \kappa_2 (\kappa_1^2 + \kappa_2^2)/\omega_B^2}$. Also, it is easy to see that the transfer function from $b_4^\dagger$ to $\tilde{b}_1$ has the same form of second-order Butterworth filter as above. Note that, as mentioned in Sec. A, the amplitude of the input field should be much bigger than that of the amplified idler vacuum noise.

Figure 11 shows the gain plot of the second-order Butterworth filter developed above. In this figure, the black solid line shows the gain plot of the ideal transfer function $G_{21}^{(FB)}(i\omega) = -K_{11}(i\omega)/K_{21}(i\omega)$, which corresponds to $\gamma \to 2\lambda + 0$, while the dotted lines show the gain plot of $G_{21}^{(FB)}(i\omega) = G_{21}(i\omega) K_{11}(i\omega)/\{1 - K_{21}(i\omega) G_{22}(i\omega)\}$ with $\gamma = 2.01\lambda$ and several parameters $\lambda = m\kappa_1$ ($m = 1, 3, 5, 7$). The other parameters are fixed to $\kappa_2 = 1.5\kappa_1$ and $\Delta = (\kappa_1 + \kappa_2)/2$. Now, as mentioned before, $|G_{11}(i\omega)| \gg 1$ holds in the frequency range $\omega \ll \gamma = 2.01\lambda$. Therefore, making λ bigger results in broadening the frequency range where the approximation is valid, and in fact Fig. 11 shows that the dotted line approaches the ideal solid line as λ gets larger.

D. Nonreciprocal amplifier

The last topic in this section is a proposal of a nonreciprocal (directional) amplifier, constructed via the feedback-amplification method. Nonreciprocal amplifiers are particularly useful in the field of superconducting circuit-based

quantum technologies [44–46]. In the microwave regime the phase-preserving amplifier obeys the same Eq. (4), but the configuration differs from the optical case; the input b_1 and the corresponding output $\tilde{b}_1$ propagate along the same transmission line yet with opposite direction as shown in Fig. 8(c). If the purpose of the use of amplifier is to detect a small signal b_1 generated from a source system, e.g., a superconducting qubit, then the propagating direction of the reflected output field $\tilde{b}_1$ must be changed to protect the source system from the backward field (if the output $\tilde{b}_1$ is the amplified vacuum noise field) or to measure it (if the output $\tilde{b}_1$ is the amplified signal). In fact there have been a number of theoretical and experimental proposals of active nonreciprocal amplifier [23–27]. Our scheme is similar to Ref. [27], but it has a clear concept of using the feedback amplification to realize a robust nonreciprocal amplifier as described below.

Before describing the result, we note that the assumptions in the coherent feedback theory (e.g., see Ref. [47]) are not always satisfied in superconducting devices, while there is certainly the case where the theory is valid and was experimentally demonstrated [48]. Here we leave this problem, i.e., the analysis for experimental implementability of the method in the proposed superconducting circuit, for the future work.

The proposed microwave nonreciprocal amplifier has a form of coherent feedback shown in Fig. 12(a), which takes into account the above-mentioned fact that the input and reflected output fields propagate along the same transmission line. This whole system has three inputs (b_1, b_3, b_4) and three outputs $(\tilde{b}_2, \tilde{b}_3, \tilde{b}_4)$; particularly b_3 is the input signal and $\tilde{b}_3$ is the amplified signal to be detected, while b_1 and b_4 are the vacuum field. G and $\overline{G}$ are both phase-preserving amplifiers, and K is a passive system. As mentioned above, the source system generating b_3 may be contaminated due to the backward field $\tilde{b}_4$, which is not necessarily vacuum. Hence $\tilde{b}_4$ should be sufficiently suppressed.

Each system component has the following input-output relations:

$$\begin{bmatrix} \tilde{b}_1(s) \\ \tilde{b}_1^\dagger(s^*) \end{bmatrix} = \begin{bmatrix} G_{11}(s) & G_{12}(s) \\ G_{21}(s) & G_{22}(s) \end{bmatrix} \begin{bmatrix} \tilde{b}_3(s) \\ b_1^\dagger(s^*) \end{bmatrix}, \quad (29)$$

$$\begin{bmatrix} \tilde{b}_2^\dagger(s^*) \\ \tilde{b}_2(s) \end{bmatrix} = \begin{bmatrix} \overline{G}_{11}(s) & \overline{G}_{12}(s) \\ \overline{G}_{21}(s) & \overline{G}_{22}(s) \end{bmatrix} \begin{bmatrix} \tilde{b}_1^\dagger(s^*) \\ b_2(s) \end{bmatrix}, \quad (30)$$

$$\begin{bmatrix} \tilde{b}_3(s) \\ \tilde{b}_3(s) \end{bmatrix} = \begin{bmatrix} K_{11}(s) & K_{12}(s) \\ K_{21}(s) & K_{22}(s) \end{bmatrix} \begin{bmatrix} b_3(s) \\ \tilde{b}_2(s) \end{bmatrix}, \quad (31)$$

$$\begin{bmatrix} \tilde{b}_4(s) \\ b_2(s) \end{bmatrix} = \begin{bmatrix} K_{11}^*(s) & K_{21}^*(s) \\ K_{12}^*(s) & K_{22}^*(s) \end{bmatrix} \begin{bmatrix} b_4(s) \\ \tilde{b}_1(s) \end{bmatrix}. \quad (32)$$
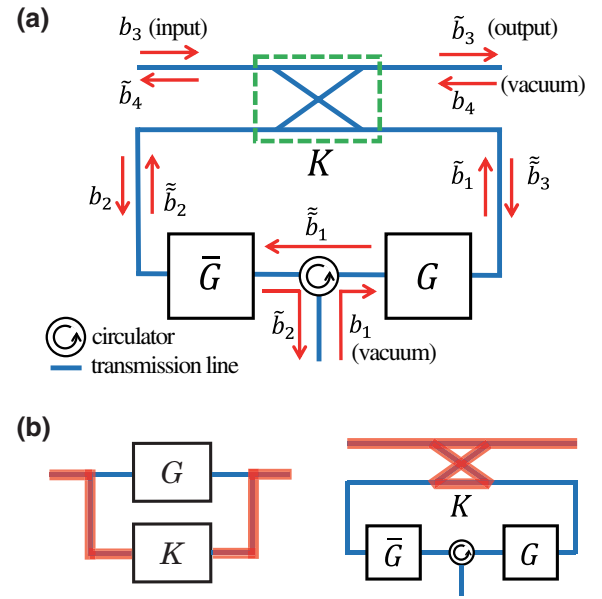

(a)

(b)

FIG. 12.   (a) Configuration of the proposed microwave nonreciprocal amplifier with the input b_3 and the amplified output $\tilde{b}_3$. This system is composed of two amplifiers (G, $\overline{G}$) and a passive controller K. Although in this figure K represents a beam splitter, other general quantum passive systems can also work as K. (b) Intuitive illustration of the signal flow in the closed-loop system containing high-gain amplifiers in the general classical case (left) and in the proposed quantum case (right).

Combining these equations, the input-output relation of the whole feedback-controlled system is represented as follows:

$$\begin{bmatrix} \tilde{b}_2^\dagger(s^*) \\ \tilde{b}_3(s) \\ \tilde{b}_4(s) \end{bmatrix} = G^{(\mathrm{FB})}(s) \begin{bmatrix} b_1^\dagger(s^*) \\ b_3(s) \\ b_4(s) \end{bmatrix},$$

$$G^{(\mathrm{FB})}(s) = \begin{bmatrix} G_{11}^{(\mathrm{FB})}(s) & G_{12}^{(\mathrm{FB})}(s) & G_{13}^{(\mathrm{FB})}(s) \\ G_{21}^{(\mathrm{FB})}(s) & G_{22}^{(\mathrm{FB})}(s) & G_{23}^{(\mathrm{FB})}(s) \\ G_{31}^{(\mathrm{FB})}(s) & G_{32}^{(\mathrm{FB})}(s) & G_{33}^{(\mathrm{FB})}(s) \end{bmatrix}. \quad (33)$$

Here we find that, in a s domain such that both $G(s)$ and $\overline{G}(s)$ have a large gain, the transfer function matrix $G^{(\mathrm{FB})}(s)$ converges to

$$G^{(\mathrm{FB})}(s) \rightarrow \begin{bmatrix} -\dfrac{1}{K_{22}(s)} & -\dfrac{K_{21}(s)}{K_{22}(s)} & 0 \\ -\dfrac{K_{12}(s)}{K_{22}(s)} & \dfrac{\det[K(s)]}{K_{22}(s)} & 0 \\ 0 & 0 & \dfrac{K_{11}^*(s) + \det[K^\dagger(s)]}{1 + K_{22}^*(s)} \end{bmatrix}, \quad (34)$$

where

$$\left| \frac{K_{11}^*(i\omega) + \det[K^\dagger(i\omega)]}{1 + K_{22}^*(i\omega)} \right| = 1, \quad \forall \omega \qquad (35)$$

holds. The proof of Eq. (34) is given in Appendix A, and Eq. (35) can be proven by using the unitary property of $K(i\omega)$ [i.e., $|K_{11}(i\omega)|^2 + |K_{12}(i\omega)|^2 = 1$, $|K_{21}(i\omega)|^2 + |K_{22}(i\omega)|^2 = 1$, and $K_{21}(i\omega)K_{11}^*(i\omega) + K_{22}(i\omega)K_{12}^*(i\omega) = 0$]. The point of this result is that, because b_4 is vacuum, the backward-field mode $\tilde{b}_4$ propagating towards the input port [see Fig. 12(a)] is also a vacuum field in this high-gain limit. This means that the noise of the backward field at the input port is suppressed to the vacuum in the feedback configuration. Therefore, because the output signal $\tilde{b}_3$ contains the input signal b_3 with amplification gain $\det[K]/K_{22}$ that depends only on the passive component, this feedback-controlled system functions as a robust nonreciprocal amplifier or more broadly a robust nonreciprocal active filter.

Let us consider an example. If K is given by a beam splitter with power transmissivity T:

$$K(s) = \begin{bmatrix} \sqrt{T} & -\sqrt{1-T} \\ \sqrt{1-T} & \sqrt{T} \end{bmatrix},$$

then we have

$$G^{(\mathrm{FB})}(s) = \begin{bmatrix} -1/\sqrt{T} & -\sqrt{1/T-1} & 0 \\ \sqrt{1/T-1} & 1/\sqrt{T} & 0 \\ 0 & 0 & 1 \end{bmatrix}.$$

Hence, the input signal b_3 is amplified with amplification gain $1/\sqrt{T}$. Furthermore, this nonreciprocal amplification is robust against the characteristic changes in the original amplifiers $(G, \overline{G})$ because the gain $1/\sqrt{T}$ is a tunable yet static quantity.

Lastly we provide a way for intuitively understanding the mechanism of nonreciprocity of the proposed amplifier. For this purpose, let us reconsider the classical feedback amplifier shown in Fig. 1. In this case, the input to the amplifier G, which is $u - Ky$, converges to zero when $G \to \infty$ due to the boundedness of the output y. This means that the signal injected to G effectively vanishes in the high-gain limit; as a result, the signal flows only along the line illustrated by the orange thick line in the left figure of Fig. 12(b). This view implies that the proposed nonreciprocal amplifier has a similar characteristic. That is, the signal fields injected to the amplifiers G and $\overline{G}$ effectively vanish (more precisely, suppressed to the vacuum field), and the signal propagates only through the passive system K as illustrated by the orange thick line in the right figure of Fig. 12(b). This is indeed a useful property, because the signal does not pass through the circulator; in fact, microwave circulators are in general noisy, and thus, developing a nonreciprocal amplifier without circulators is what

has been pursued recently [23–27]. Therefore, it would be interesting to conduct an experiment to see how much the signals injected to the amplifiers G and $\overline{G}$ are suppressed.

VIII. APPLICATION TO GRAVITATIONAL-WAVE DETECTION

As noted before, any functionality realized via the feedback amplification method should be evaluated in such a way that it is incorporated in a concrete setup with particular engineering purpose, to see its actual performance under practical constraints. Here we study the phase-cancellation filter discussed in Sec. B, and see how much it might broaden the bandwidth of the typical gravitational-wave detector.

A. Basics of gravitational-wave detector

The most basic schematic of the gravitational-wave detector, particularly the one that uses a laser interferometer [49–52], is shown in Fig. 13. The input laser with frequency ω_0 is injected to the arm cavities through the power-recycling mirror (PRM). Each arm cavity is composed of two mirrors: the input test mass (ITM) and the end test mass (ETM). A tidal force of gravitational-wave F_{GW} with frequency Ω induces a pendulum motion of ETMs. Then the arm cavities create the signal light fields with frequency $\omega_0 + \Omega$, which are combined at the center half mirror and leak to outside through the signal-recycling mirror (SRM); this output field is denoted as d_{out}. Note that a vacuum field d_{in} unavoidably enters into the system at SRM.

The Hamiltonian of the entire system, in the rotating frame at frequency ω_0, is given by [28,53]

$$H = \frac{P^2}{2M} + \hbar\Delta_d d^\dagger d - \hbar G_{\mathrm{arm}}(d + d^\dagger)X - F_{\mathrm{GW}}X.$$
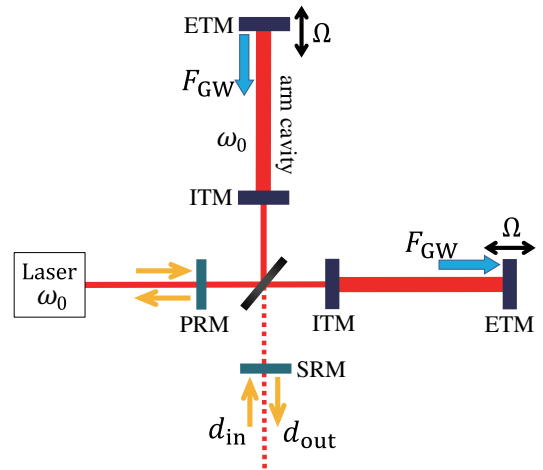

FIG. 13. Schematic of the basic gravitational-wave detector.

(X, P) are the differential (position, momentum) operators of ETMs, and they satisfy $[X(t), P(t)] = i\hbar$. M is the mass of ETMs. d is the sideband mode of the interferometer field, with detuning Δ_d, which satisfies $[d(t), d^\dagger(t)] = 1$. G_{arm} represents the coupling strength between X and d, and it is given by $G_{\text{arm}} = \sqrt{2P_{\text{arm}}\omega_0/(\hbar c L_{\text{arm}})}$ with P_{arm} the arm cavity power [28]. Then the dynamics of the system is given by

$$\dot{X} = \frac{1}{M}P, \quad \dot{P} = \hbar G_{\text{arm}}(d + d^\dagger) + F_{\text{GW}},$$

$$\dot{d} = -\left(i\Delta_d + \frac{\gamma_{\text{IFO}}}{2}\right)d + iG_{\text{arm}}X - \sqrt{\gamma_{\text{IFO}}}d_{\text{in}},$$

where γ_{IFO} (IFO stands for interferometer) is the coupling between d and d_{in}. Also, the output equation of the system is given by

$$d_{\text{out}} = \sqrt{\gamma_{\text{IFO}}}d + d_{\text{in}}.$$

Note that $[d_{\text{in}}(t), d_{\text{in}}^\dagger(t')] = [d_{\text{out}}(t), d_{\text{out}}^\dagger(t')] = \delta(t - t')$. The input-output relation in the Laplace domain, in terms of the quadratures $Q_d^{\text{in,out}} = (d_{\text{in,out}} + d_{\text{in,out}}^\dagger)/\sqrt{2}$ and $P_d^{\text{in,out}} = (d_{\text{in,out}} - d_{\text{in,out}}^\dagger)/\sqrt{2}i$, is obtained as

$$\begin{bmatrix} Q_d^{\text{out}}(s) \\ P_d^{\text{out}}(s) \end{bmatrix} = J(s) \begin{bmatrix} F_{\text{GW}}(s) \\ Q_d^{\text{in}}(s) \\ P_d^{\text{in}}(s) \end{bmatrix},$$

with

$$J(s) = \begin{bmatrix} J_{11}(s) & J_{12}(s) & J_{13}(s) \\ J_{21}(s) & J_{22}(s) & J_{23}(s) \end{bmatrix},$$

$$= \begin{bmatrix} 0 & \dfrac{s - \gamma_{\text{IFO}}/2}{s + \gamma_{\text{IFO}}/2} & 0 \\[2ex] \dfrac{\sqrt{2\gamma_{\text{IFO}}}G_{\text{arm}}}{Ms^2(s + \gamma_{\text{IFO}}/2)} & \dfrac{-2\hbar G_{\text{arm}}^2\gamma_{\text{IFO}}}{Ms^2(s + \gamma_{\text{IFO}}/2)^2} & \dfrac{s - \gamma_{\text{IFO}}/2}{s + \gamma_{\text{IFO}}/2} \end{bmatrix},$$

where $\Delta_d = 0$ is assumed. The gravitational-wave strain signal h, which is defined as $F_{\text{GW}}(t) = ML_{\text{arm}}\ddot{h}(t)$, can be detected by homodyne measuring P_d^{out}. The quantum noise operator is then defined as

$$F_N(s) = \frac{P_d^{\text{out}}(s)}{ML_{\text{arm}}s^2 J_{21}(s)} - h(s),$$

$$= \Xi_Q(s)Q_d^{\text{in}}(s) + \Xi_P(s)P_d^{\text{in}}(s), \quad (36)$$

where

$$\Xi_Q(s) = -\frac{\sqrt{2\gamma_{\text{IFO}}}\hbar G_{\text{arm}}}{ML_{\text{arm}}s^2(s + \gamma_{\text{IFO}}/2)},$$

$$\Xi_P(s) = \frac{s - \gamma_{\text{IFO}}/2}{\sqrt{2\gamma_{\text{IFO}}}G_{\text{arm}}L_{\text{arm}}}.$$

Hence $F_N(s)$ is composed of the radiation pressure noise $\Xi_Q(s)Q_d^{\text{in}}(s)$ and the shot noise $\Xi_P(s)P_d^{\text{in}}(s)$, which are
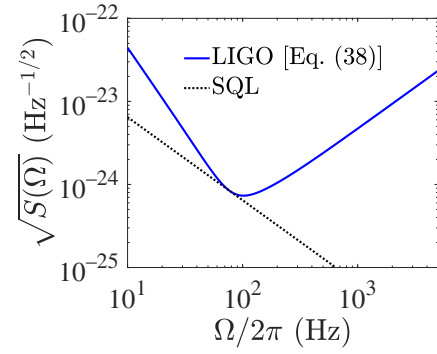

FIG. 14. Quantum noise in the basic gravitational-wave detector (blue line). The black dashed line denotes SQL.

dominant in the low- and high-frequency range, respectively. The magnitude of $F_N(i\Omega)$ is quantified by the spectral density $S(\Omega)$, which is generally defined by [54–56]

$$2\pi S(\Omega)\delta(\Omega - \Omega')$$

$$= \left\langle F_N(i\Omega)F_N^\dagger(i\Omega') + F_N^\dagger(i\Omega')F_N(i\Omega) \right\rangle/2. \quad (37)$$

It is now calculated as

$$S(\Omega) = \left[\left|\Xi_Q(i\Omega)\right|^2 + \left|\Xi_P(i\Omega)\right|^2\right]/2, \quad (38)$$

which is lower bounded by the standard quantum limit (SQL) [53,57,58]: $S_{\text{SQL}}(\Omega) = \left|\Xi_Q\Xi_P\right| = \hbar/(ML_{\text{arm}}^2\Omega^2)$. Note that, however, there have been several proposals to beat SQL, which can be now even experimentally observed in the real LIGO system [59]. Figure 14 shows the sensitivity $\sqrt{S(\Omega)}$ in the following typical setup [29,57]: $M = 40$ kg, $L_{\text{arm}} = 4$ km, $P_{\text{arm}} = 800$ kW, $\omega_0 = 2\pi c/\lambda_{\text{laser}}$, $\lambda_{\text{laser}} = 1064$ nm, $\Delta_d = 0$, $\gamma_{\text{IFO}} = 2\pi \times 200$ Hz. Also recall that Ω is the gravitational-wave frequency.

B. Effect of the phase-cancellation filter

As seen above, the detection sensitivity (roughly the inverse of the noise magnitude) is limited by the quantum noise. Particularly, the following equality holds [60], meaning that there is a trade-off between the bandwidth and the peak sensitivity:

$$\int_0^\infty \frac{1}{\left|\Xi_P(i\Omega)\right|^2}d\Omega = 2\pi G_{\text{arm}}^2 L_{\text{arm}}^2.$$

In fact, because the integral does not depend on the bandwidth of the cavity, γ_{IFO}, a broad-band enhancement of the sensitivity is not allowed.

As described in Sec. B, the above trade-off is attributed to the frequency-dependent propagation phase $\phi_{\text{arm}}(\Omega) = -2\Omega L_{\text{arm}}/c$. The idea proposed in Ref. [28] is to construct the phase-cancellation filter with transfer function

$e^{-i\phi_{\text{arm}}(\Omega)} = e^{2i\Omega L_{\text{arm}}/c}$ to compensate $\phi_{\text{arm}}(\Omega)$. Now, unlike the optomechanics-based scheme proposed in Ref. [28], we can construct the same filter, Eq. (27), in an all-optics setup, using the feedback-amplification method. Figure 15(b) shows $\phi_{\text{arm}}(\Omega)$ and

$$\phi_G = \arg\left[G_{11}^{(\text{FB})}(i\Omega)\right] = \arg\left[\frac{G_{11} - K_{21}\det[G]}{1 - K_{21}G_{22}}\right], \quad (39)$$

where G is the transfer function of NDPA and K is given by Eq. (10) with $\Delta = \kappa_2 = 0$; this approximates $-\phi_{\text{arm}}$ in the high-gain limit, as proven in Eq. (27). The parameters are set as $L_{\text{arm}} = 4$ km, $\lambda = 3 \times 10^6$ Hz, $\gamma = 2.01\lambda$, and $\kappa_1 = 2c/L_{\text{arm}}$. We can see from Fig. 15(b) that the filter certainly achieves the desired phase cancellation in the frequency
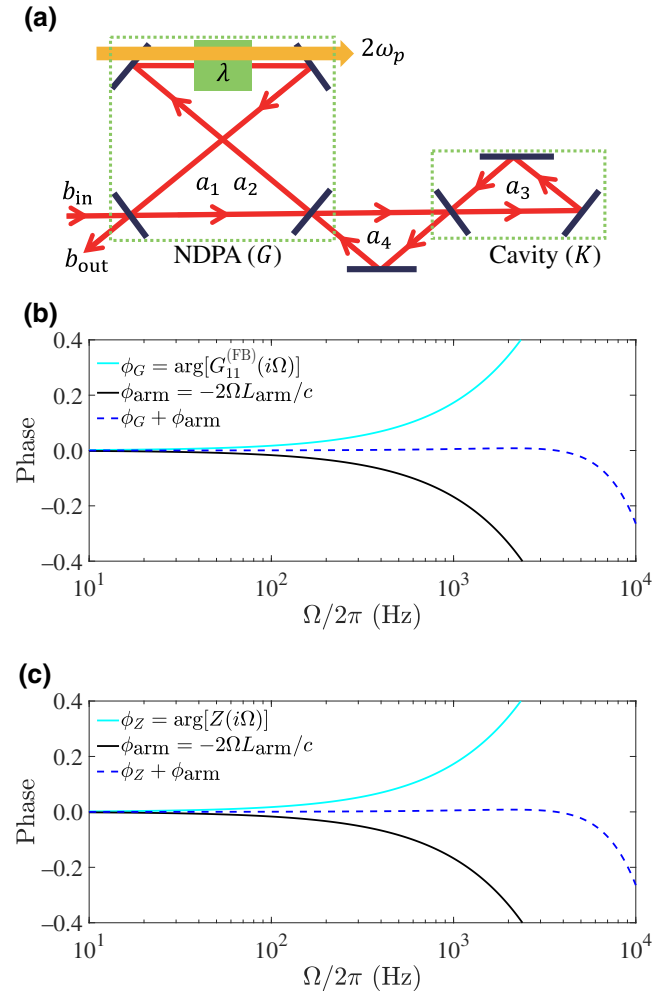
(a)

(b)

(c)

FIG. 15. (a) Configuration of the phase-cancellation filter, where the feedback loop between the amplifier and the cavity is regarded as another cavity with mode a_4. (b) Phase plot of the phase-cancellation filter $G_{11}^{(\text{FB})}(i\Omega)$ in Eq. (39) together with $\phi_{\text{arm}}(\Omega)$. (c) Phase of the phase-cancellation filter $Z(i\Omega)$ in Eq. (40) together with $\phi_{\text{arm}}(\Omega)$.

range where $\Omega \ll \kappa_1 = 2c/L_{\text{arm}} \approx 2\pi \times 2.39 \times 10^4$ Hz is satisfied.

Now recall that the filter is realized as the feedback-controlled system shown in Fig. 15(a). That is, as discussed in the case of the integrator in Sec. B, the feedback loop between the amplifier (G) and the cavity (K) forms a loop cavity with mode a_4. The total Hamiltonian of the filter is given by Eq. (20), and we again assume $\omega_k = \omega_p$ ($k = 1, \ldots, 4$). Then in the rotating frame at frequency ω_p, the dynamics and output equation of the filter are given by

$$\dot{a}_1 = -\frac{\gamma}{2}a_1 + \lambda a_2^\dagger - \sqrt{\gamma}b_{\text{in}}, \quad \dot{a}_2^\dagger = \lambda a_1 + ig_{24}a_4^\dagger,$$

$$\dot{a}_3^\dagger = ig_{34}a_4^\dagger, \quad \dot{a}_4^\dagger = ig_{24}a_2^\dagger + ig_{34}a_3^\dagger,$$

$$b_{\text{out}} = \sqrt{\gamma}a_1 + b_{\text{in}},$$

with $g_{24} = \sqrt{c\gamma/L_4}$ and $g_{34} = \sqrt{c\kappa_1/L_4}$. This equation is the same as Eq. (22) except that control cavity K couples to only the loop cavity. The input-output relation of this system in the Laplace domain is represented as

$$b_{\text{out}}(s) = Z(s)b_{\text{in}}(s),$$

$$Z(s) = \frac{s^4 + \alpha_3 s^3 + \alpha_2 s^2 + \alpha_1 s + \alpha_0}{s^4 + \beta_3 s^3 + \beta_2 s^2 + \beta_1 s + \beta_0}, \quad (40)$$

where

$$\alpha_3 = -\gamma/2, \quad \alpha_2 = g_{24}^2 + g_{34}^2 - \lambda^2,$$

$$\alpha_1 = -(g_{24}^2 + g_{34}^2)\gamma/2,$$

$$\alpha_0 = -\lambda^2 g_{24}^2, \quad \beta_3 = \gamma/2, \quad \beta_2 = g_{24}^2 + g_{34}^2 - \lambda^2,$$

$$\beta_1 = (g_{24}^2 + g_{34}^2)\gamma/2, \quad \beta_0 = -\lambda^2 g_{34}^2.$$

Now we show that $Z(i\Omega)$ approximates the target phase-cancellation filter $e^{2i\Omega L_{\text{arm}}/c}$ in the high-gain limit $\gamma \to 2\lambda + 0$. First, by setting $\kappa_1 = 2c/L_{\text{arm}}$ and taking this limit, the coefficients in $Z(s)$ become

$$\alpha_3 = -\beta_3 = -\lambda, \quad \alpha_2 = \beta_2 = \frac{2c(c + L_{\text{arm}}\lambda)}{L_{\text{arm}}L_4} - \lambda^2,$$

$$\alpha_1 = -\beta_1 = -\frac{2c\lambda(c + L_{\text{arm}}\lambda)}{L_{\text{arm}}L_4}, \quad \alpha_0 = \beta_0 = -\frac{2c^2\lambda^2}{L_{\text{arm}}L_4}.$$

Then, in the s domain with $|s| \ll \gamma$, or equivalently $|s| \ll \lambda$, we have

$$Z(s) \approx \frac{\alpha_1 s + \alpha_0}{\beta_1 s + \beta_0} = -\frac{s + \dfrac{c\lambda}{c + L_{\text{arm}}\lambda}}{s - \dfrac{c\lambda}{c + L_{\text{arm}}\lambda}}.$$

Now we set an additional assumption $\kappa_1 \ll \gamma$, which leads to $c \ll L_{\text{arm}}\lambda$ and as a result

$$Z(s) \approx -\frac{s + c/L_{\text{arm}}}{s - c/L_{\text{arm}}}.$$

This is exactly the same as the transfer function $G_{11}^{(FB)}(s)$ in Eq. (26) with $\kappa_1 = 2c/L_{arm}$. Hence $Z(i\Omega) \approx e^{2i\Omega L_{arm}/c} = e^{-i\phi_{arm}(\Omega)}$ holds, meaning that the system depicted in Fig. 15(a) may approximate the target phase-cancellation filter. This can be actually seen in Fig. 15(c) showing the phase plot of $Z(i\Omega)$ given in Eq. (40), where $L_4 = 0.5$ m and the other parameters are the same as those used in Fig. 15(b). This shows that the exact model incorporating the loop cavity a_4 certainly has the desired phase-canceling effect.

C. The entire system and stabilizing control

In the previous subsection we see that the constructed filter certainly has a desired phase-cancellation property, from which we expect that this active filter broadly enhances the sensitivity of the gravitational-wave detector in the high-frequency regime. Here we model the entire system composed of the interferometer and the phase-cancellation filter depicted in Fig. 16. This entire system must be stabilized, because the phase cancellation filter is itself an unstable system; here we employ measurement-based feedback for this purpose.

Note that this measurement feedback is not an additional requirement over the existing proposals; the stabilization is necessary as well in the optomechanics-based implementation [28,29].

Let us begin with the dynamics of the entire system without stabilization. Here we assume that $\omega_p = \omega_k = \omega_0$ ($k = 1, \ldots, 4$). Then in the rotating frame at frequency ω_0, the Hamiltonian of the entire system is given by
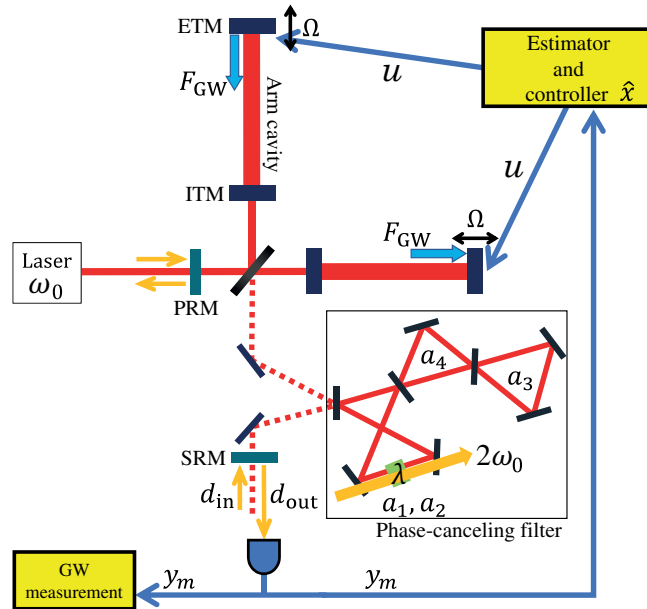
$$H_{tot} = \frac{P^2}{2M} + \Delta_d d^\dagger d - \hbar G_{arm}(d + d^\dagger)X - F_{GW}X$$
$$+ \hbar g_{NI}(d^\dagger a_1 + d a_1^\dagger) + i\hbar\lambda(a_1^\dagger a_2^\dagger - a_1 a_2)$$
$$+ \hbar g_{24}(a_2^\dagger a_4 + a_2 a_4^\dagger) + \hbar g_{34}(a_3^\dagger a_4 + a_3 a_4^\dagger),$$

where again (X, P) are the differential (position, momentum) operators of ETMs, d is the sideband mode of the interferometer field and NI stands for NDPA and interferometer. We assume that only a_1 couples with d, with strength $g_{NI} = \sqrt{c\gamma/(2L_{arm})}$. The signal leaks to outside through the SRM where the vacuum input d_{in} must enter. Then the dynamical equation of the entire system is given by

$$\dot{X} = \frac{1}{M}P, \quad \dot{P} = \hbar G_{arm}(d + d^\dagger) + F_{GW},$$

$$\dot{d} = -i\Delta_d d - \frac{\gamma_{IFO}}{2}d + iG_{arm}X - ig_{NI}a_1 - \sqrt{\gamma_{IFO}}d_{in},$$

$$\dot{a}_1 = -\frac{\gamma_{1loss}}{2}a_1 - ig_{NI}d + \lambda a_2^\dagger - \sqrt{\gamma_{1loss}}b_{1loss},$$

$$\dot{a}_2 = \lambda a_1^\dagger - ig_{24}a_4, \quad \dot{a}_3 = -\frac{\kappa_{3loss}}{2}a_3 - ig_{34}a_4$$
$$- \sqrt{\kappa_{3loss}}b_{3loss},$$

$$\dot{a}_4 = -\frac{\kappa_{4loss}}{2}a_4 - ig_{24}a_2 - ig_{34}a_3 - \sqrt{\kappa_{4loss}}b_{4loss},$$

$$d_{out} = \sqrt{\gamma_{IFO}}d + d_{in},$$

where b_{kloss} ($k = 1, 3, 4$) are the noise field representing the optical losses of the internal modes a_k with magnitude κ_{kloss}. We use the quadrature representation $q_k = (a_k + a_k^\dagger)/\sqrt{2}$, $p_k = (a_k - a_k^\dagger)/(\sqrt{2}i)$ ($k = d, 1, 2, 3, 4$), $Q_d^{in,out} = (d_{in,out} + d_{in,out}^\dagger)/\sqrt{2}$, $P_d^{in,out} = (d_{in,out} - d_{in,out}^\dagger)/(\sqrt{2}i)$, $Q_{nloss} = (b_{nloss} + b_{nloss}^\dagger)/\sqrt{2}$, $P_{nloss} = (b_{nloss} - b_{nloss}^\dagger)/(\sqrt{2}i)$ ($n = 1, 3, 4$). Also we define the dimensionless operators $X_M = X\sqrt{M\Omega_M/\hbar}$ and $P_M = P/\sqrt{\hbar M\Omega_M}$, with Ω_M the eigenfrequency of the ETM; they satisfy $[X_M, P_M] = i$. Then the above dynamical equations are summarized to

$$\dot{x} = Ax + B_w w, \quad y = Cx + Dw,$$

where $x = [\, X_M \; P_M \; q_d \; p_d \; q_1 \; p_1 \; q_2 \; p_2 \; q_3 \; p_3 \; q_4 \; p_4 \,]^T$, $w = [\, F_{GW} \; Q_d^{in} \; P_d^{in} \; Q_{1loss} \; P_{1loss} \; Q_{3loss} \; P_{3loss} \; Q_{4loss} \; P_{4loss} \,]^T$, and $y = [\, Q_d^{out} \; P_d^{out} \,]^T$. The matrices $A \in \mathbb{R}^{12\times12}$, $B_w \in \mathbb{R}^{12\times9}$, $C \in \mathbb{R}^{2\times12}$, $D \in \mathbb{R}^{2\times9}$ are shown in Appendix B. Note that A has eigenvalues with positive real part, meaning that the uncontrolled entire system is unstable.

To stabilize the system, we apply the measurement-based quantum feedback control, particularly the quantum linear quadratic Gaussian (LQG) feedback control [34], which has the same form as the classical version [61]. This control is generally conducted by feeding a measurement

FIG. 16. Structure of the entire controlled system.

output back to control the system. In our case we measure P_d^{out} by the photodetector (note that measuring both Q_d^{out} and P_d^{out} is prohibited by quantum mechanics); the measurement result is used to construct the estimate $\hat{x}$, which is fed back to control the ETMs directly by implementing a piezoactuator [62]. This control is modeled by adding the classical input $u = -F_u\hat{x}$ to the dynamics of the oscillator, where $F_u \in \mathbb{R}^{1\times12}$ is the feedback gain to be designed. In the LQG setting, the (quantum) Kalman filter is used to obtain the least-squared estimate $\hat{x}$. The entire controlled system is then given by

$$
\begin{aligned}
\dot{x} &= Ax + B_w w + B_u u, \\
y_m &= P_d^{\text{out}} = C_m x + D_m w, \\
\dot{\hat{x}} &= A\hat{x} + B_u u + K_u(y_m - C_m\hat{x}), \quad u = -F_u\hat{x},
\end{aligned}
\tag{41}
$$

where $K_u \in \mathbb{R}^{12}$ is the Kalman gain shown later. $B_u = [0, 1, 0, \ldots, 0]^T \in \mathbb{R}^{12}$ (only the second element is nonzero) represents that the actuator directly drives P_M of the oscillator. $C_m \in \mathbb{R}^{1\times12}$ and $D_m \in \mathbb{R}^{1\times9}$ are second row vectors of C and D, respectively. Here we define $e = \hat{x} - x$. Then the above dynamical equation is rewritten as

$$
\begin{bmatrix} \dot{x} \\ \dot{e} \end{bmatrix} = A_{\text{tot}} \begin{bmatrix} x \\ e \end{bmatrix} + B_{\text{tot}}w, \quad y_m = C_{\text{tot}} \begin{bmatrix} x \\ e \end{bmatrix} + D_{\text{tot}}w,
$$

where

$$
A_{\text{tot}} = \begin{bmatrix} A - B_u F_u & -B_u F_u \\ 0 & A - K_u C_m \end{bmatrix}, \quad C_{\text{tot}} = \begin{bmatrix} C_m & 0 \end{bmatrix},
$$

$$
B_{\text{tot}} = \begin{bmatrix} B_w \\ K_u D_m - B_w \end{bmatrix}, \quad D_{\text{tot}} = D_m.
$$

The entire system becomes stable when A_{tot} has no eigenvalue with positive real part. Since the eigenvalues of A_{tot} are the same as those of $A - B_u F_u$ and $A - K_u C_m$, we can stabilize the system by determining appropriate F_u and K_u. The necessary and sufficient condition for such F_u and K_u to exist is that the system is controllable and observable; that is, the following controllability matrix $\mathcal{C}_u$ and observability matrix $\mathcal{O}_{y_m}$ are of full rank:

$$
\begin{aligned}
\mathcal{C}_u &= \begin{bmatrix} B_u & AB_u & \cdots & A^{11}B_u \end{bmatrix}, \\
\mathcal{O}_{y_m} &= \begin{bmatrix} C_m^T & A^T C_m^T & \cdots & (A^T)^{11}C_m^T \end{bmatrix}^T.
\end{aligned}
\tag{42}
$$

In the LQG setup, F_u and K_u are determined from the policy to minimize the following cost function $\mathcal{J}$ and the estimation error ϵ:

$$
\begin{aligned}
\mathcal{J} &= \lim_{t\to\infty} \frac{1}{t} \Big\langle \int_0^t \big[x^T(\tau)Qx(\tau) + Ru^2(\tau) \big] d\tau \Big\rangle, \\
\epsilon &= \big\langle (x - \hat{x})^T (x - \hat{x}) \big\rangle,
\end{aligned}
\tag{43}
$$

where $Q \in \mathbb{R}^{12\times12}$ and $R \in \mathbb{R}$ are the weighing matrices. From the separation principle of the LQG control,

these two optimization problems can be solved separately. If the optimal solutions of F_u and K_u are uniquely determined, then they stabilize the entire system and are given by

$$
F_u = R^{-1}B_u^T P_F, \quad K_u = (P_K C_m^T + B_w V D_m^T)(D_m D_m^T)^{-1},
$$

where $P_F \in \mathbb{R}^{12\times12}$ and $P_K \in \mathbb{R}^{12\times12}$ are the solutions of the following algebraic Riccati equations:

$$
\begin{aligned}
&P_F A + A^T P_F - P_F B_u R^{-1} B_u^T P_F + Q = 0, \\
&P_K A^T + A P_K + B_w V B_w^T - (P_K C_m^T + B_w V D_m^T) \\
&\quad \times (D_m V D_m^T)^{-1}(P_K C_m^T + B_w V D_m^T)^T = 0.
\end{aligned}
$$

V is the covariance matrix of the vector w. Note that F_{GW}, the first element of w, is assumed to be a Gaussian noise with known variance, but in reality it is an unknown signal whose noise part is not necessarily Gaussian; as we describe later, this assumption can be weakened so that only a stabilizing controller exists.

D. Quantum noise of the stabilized system

The quantum noise observed at the detector is calculated as follows. First we have

$$
\begin{aligned}
y_m(s) &= \big[C_{\text{tot}}(sI - A_{\text{tot}})^{-1}B_{\text{tot}} + D_{\text{tot}} \big] w(s), \\
&= \Psi_{Q_d}(s)Q_d^{\text{in}}(s) + \Psi_{P_d}(s)P_d^{\text{in}}(s) + \Psi_h(s)h(s) \\
&\quad + \sum_{k=1,3,4} \big[\Psi_{Q_k}(s)Q_{k\text{loss}}(s) + \Psi_{P_k}(s)P_{k\text{loss}}(s) \big],
\end{aligned}
$$

where the functions $\Psi_\star$ are the transfer functions from the corresponding noise fields and the gravitational-wave strain signal $h(t)$ to the output y_m. As shown in Eq. (36), the quantum noise operator is defined as $F_N(i\Omega) = y_m(i\Omega)/\Psi_h(i\Omega) - h(i\Omega)$. Then from Eq. (37), we obtain the noise spectral density:

$$
\begin{aligned}
S(\Omega) = \frac{1}{2|\Psi_h|^2} \Big(&|\Psi_{Q_d}|^2 + |\Psi_{P_d}|^2 + |\Psi_{Q_1}|^2 + |\Psi_{P_1}|^2 \\
&+ |\Psi_{Q_3}|^2 + |\Psi_{P_3}|^2 + |\Psi_{Q_4}|^2 + |\Psi_{P_4}|^2 \Big).
\end{aligned}
$$

The value of parameters chosen in this study are shown in Table I. For the interferometer part, unlike the setup in Fig. 14, a nonzero value of Δ_d is taken, which is necessary for the system to be controllable and observable; actually $\mathcal{C}_u$ and $\mathcal{O}_{y_m}$ in Eq. (42) are both of full rank in these parameter choice. This nonzero value of Δ_d and the value of γ_{IFO} are calculated from the scaling law [57,63] of the gravitational-wave detector containing a SRM; consequently the coupling constant γ_{IFO} is effectively changed to 1062 Hz from $2\pi \times 200$ Hz. For the phase-cancellation

TABLE I.　Parameters used in Sec. VIII. The parameters $\gamma_{1\text{loss}}$, $\kappa_{4\text{loss}}$, and $\kappa_{3\text{loss}}$ change in Figs. 18(a)–18(c), respectively. Note that $\kappa_1 = 2c/L_{\text{arm}}$ draws the connection between the GW interferometer and the phase-cancellation filter.

	Symbol	Definition	Value
GW interferometer	M	Mass of ETMs	40 kg
	L_{arm}	Arm cavity length	4 km
	P_{arm}	Arm cavity power	800 kW
	Ω_M	Mechanical frequency of ETMs	1 Hz
	λ_{laser}	Laser wavelength	1064 nm
	ω_0	Laser frequency	$= 2\pi c/\lambda_{\text{laser}}$
	Δ_d	Effective detuning	≈ -63 Hz
	γ_{IFO}	Effective coupling constant between d and d_{in}	≈ 1062 Hz
Phase-cancellation filter	λ	Coupling strength between a_1 and a_2	3×10^6 Hz
	γ	Coupling strength between the modes in NDPA and the external itinerant fields	$= 2.01\lambda$
	κ_1	If a_4 was an itinerant field, it represents the coupling strength between a_3 and a_4	$= 2c/L_{\text{arm}}$
	L_4	Round-trip cavity length of the cavity with the mode a_4	0.5 m
	g_{24}	Coupling strength between a_2 and a_4	$= \sqrt{c\gamma/L_4}$
	g_{34}	Coupling strength between a_3 and a_4	$= \sqrt{c\kappa_1/L_4}$
	$\gamma_{1\text{loss}}$	Loss magnitude of the modes in NDPA	1 MHz
	$\kappa_{3\text{loss}}$	Loss magnitude of a_3	100 Hz
	$\kappa_{4\text{loss}}$	Loss magnitude of a_4	600 kHz
Stabilizer	Q	Regulator weights for the state x	I
	R	Regulator weights for the input u	0.01
	V	Covariance matrix	diag$\{10^{-22}, 1/2, \cdots, 1/2\}$

filter part, we emphasize that $\kappa_1 = 2c/L_{\text{arm}}$ is the condition to cancel the phase and it draws the connection between the interferometer and the phase-cancellation filter. For the LQG controller part, the value of 1/2 in $V = \text{diag}\{10^{-22}, 1/2, \ldots, 1/2\}$ [all 1/2 except the $(1, 1)$ element] denotes the vacuum fluctuation. On the other hand, the $(1, 1)$ element of V denotes the variance of F_{GW}, which is unknown as mentioned at the end of the previous subsection. Hence we use Fig. 1 in Ref. [49] to have an estimate value 10^{-22}, meaning that the Kalman filter does not produce the optimal estimate $\hat{x}$. However, note that we do not need a very accurate estimate of this value but require the LQG control only to stabilize the entire control system. In fact with the above parameter choice, this purpose is fulfilled, and we end up with Fig. 17; this shows that the proposed phase-cancellation filter can enhance the bandwidth in the high-frequency regime without sacrificing the peak sensitivity.

We conclude this section with discussion on the possible advantages and disadvantages of the proposed filter. Figures 18(a) and 18(b) show the quantum noise of the entire controlled system with several optical-loss magnitudes in (a) NDPA and (b) the loop cavity. Recall that the loss magnitude of the cavity modes are represented as $\gamma_{1\text{loss}} = cT_{1\text{loss}}/L_1$ and $\kappa_{4\text{loss}} = cT_{4\text{loss}}/L_4$, where $(T_{1\text{loss}}, T_{4\text{loss}})$ and (L_1, L_4) are the optical-loss ratios and the round-trip cavity

lengths of the corresponding cavity modes, respectively. In the figures, the cavity lengths are fixed to $L_1 = 1.5$ m and $L_4 = 0.5$ m, and we change optical-loss ratios to plot the noise spectral densities with several loss magnitudes $\gamma_{1\text{loss}}$ or $\kappa_{4\text{loss}}$. The other parameters are the same as those used in Fig. 17. The figures show that the sensitivity is not largely affected by the optical losses both in NDPA ($\gamma_{1\text{loss}}$) and the loop cavity ($\kappa_{4\text{loss}}$). In particular, the loss in the loop
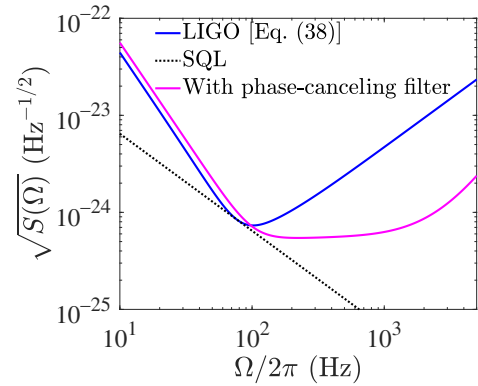

FIG. 17.　Quantum noise spectral density of the controlled gravitational-wave detector, containing the phase-cancellation filter.

cavity has almost no effect on the sensitivity, as expected from the fact that the feedback-amplification scheme is in general robust against the imperfection in the feedback loop [6]. As for the loss in NDPA, there is certainly some impact on the sensitivity in the high-frequency regime, but this can be reduced by making the length of NDPA longer.

On the other hand, the parameter $\kappa_{3\text{loss}}$, i.e., the optical-loss magnitude in the control cavity with mode a_3, has a large impact on the sensitivity, as indicated in Fig. 18(c); note that the parameters other than $\kappa_{3\text{loss}}$ are the same as

FIG. 18. Quantum noise of the controlled gravitational-wave detector with several optical-loss magnitudes of (a) the NDPA $\kappa_{1\text{loss}}$, (b) the loop cavity $\kappa_{4\text{loss}}$, and (c) the control cavity $\kappa_{3\text{loss}}$.

those used in Fig. 17. Figure 18(c) shows why $\kappa_{3\text{loss}}$ is chosen to be much smaller than $\gamma_{1\text{loss}}$ and $\kappa_{4\text{loss}}$ in Fig. 17. To achieve such a small loss, the optical path length of the control cavity should be long; from $\kappa_{3\text{loss}} = cT_{3\text{loss}}/L_3$ with $T_{3\text{loss}}$ the loss ratio and L_3 the round-trip length of the control cavity, if $\kappa_{3\text{loss}} = 100$ Hz is required, we need, e.g., $T_{3\text{loss}} = 0.01\%$ and $L_3 = 300$ m. That is, although the proposed phase-cancellation filter based on the feedback-amplification method can be constructed in an all-optics way in contrast to the optomechanical proposal [28], a very careful fabrication for the control cavity is required. In fact, to experimentally implement the proposed all-optics phase-cancellation filter requires a number of phase locks around the devices [64,65]; also note that the large power level of the laser injected to the interferometer is required.

IX. CONCLUSION

In this paper, we show that a variety of quantum functionalities are generated under the concept of feedback amplification. We hope that, combined with the several established quantum-information methods such as entanglement generation [66] and analog information processing [67], those basic functionalities may be effectively applied to enhance the performance of existing quantum technological devices and moreover to create a useful quantum-mechanical machine.

ACKNOWLEDGMENTS

APPENDIX A: PROOF OF EQ. (34)

The proof is composed of the following four steps.

Step 1: Derive the relation between (b_1, b_2, b_3) and $(\tilde{b}_1, \tilde{b}_2, \tilde{b}_3)$ by using Eqs. (29)–(31). More precisely, we find the transfer function $H(s)$ that satisfies the following relation:

$$\begin{bmatrix} \tilde{b}_1(s) \\ \tilde{b}_2^\dagger(s^*) \\ \tilde{b}_3(s) \end{bmatrix} = H(s) \begin{bmatrix} b_1^\dagger(s^*) \\ b_2(s) \\ b_3(s) \end{bmatrix}, \qquad (A1)$$

$$H(s) = \begin{bmatrix} H_{11}(s) & H_{12}(s) & H_{13}(s) \\ H_{21}(s) & H_{22}(s) & H_{23}(s) \\ H_{31}(s) & H_{32}(s) & H_{33}(s) \end{bmatrix}. \qquad (A2)$$
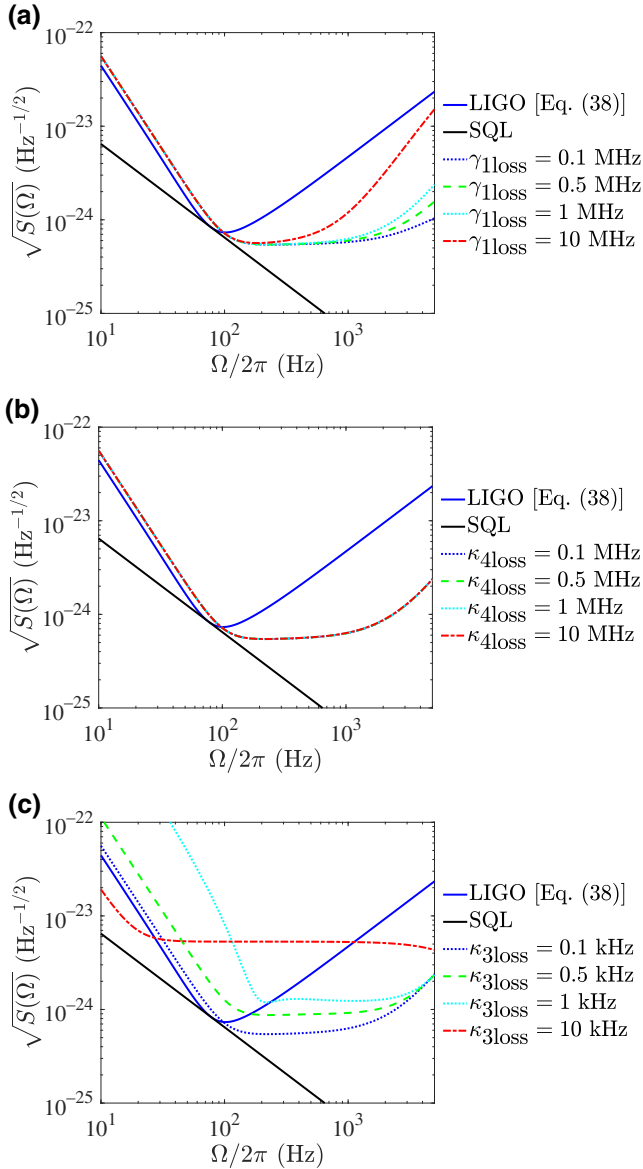
Step 2: Prove that, in the high-gain limit regime,

$$H(s) \to \begin{bmatrix} 0 & -1 & 0 \\ -1/K_{22}(s) & 0 & -K_{21}(s)/K_{22}(s) \\ -K_{12}(s)/K_{22}(s) & 0 & \det[K(s)]/K_{22}(s) \end{bmatrix}.$$

(A3)

Step 3: Derive the relation between $(\tilde{b}_2, \tilde{b}_3, \tilde{b}_4)$ and (b_1, b_3, b_4) using Eqs. (32), (A1), and (A2). That is, we aim to have the expression of $G^{(\mathrm{FB})}(s)$ in terms of $\{H_{ij}(s)\}$ and $\{K_{ij}^*(s)\}$.

Step 4: Substitute $\{H_{ij}(s)\}$ in Eq. (A3) to $\{G_{ij}^{(\mathrm{FB})}(s)\}$ obtained in step 3, which leads to Eq. (34).

First, in step 1, from Eqs. (29)–(31), the entries in $H(s)$ are found to be

$$H_{11} = \frac{G_{12} - \overline{G}_{21} K_{22} \det[G]}{1 - \overline{G}_{21} G_{21} K_{22}}, \quad H_{12} = \frac{G_{11}\overline{G}_{22} K_{22}}{1 - \overline{G}_{21} G_{21} K_{22}},$$

$$H_{13} = \frac{G_{11} K_{21}}{1 - \overline{G}_{21} G_{21} K_{22}}, \quad H_{21} = \frac{\overline{G}_{11} G_{22}}{1 - \overline{G}_{21} G_{21} K_{22}},$$

$$H_{22} = \frac{\overline{G}_{12} + G_{21} K_{22} \det[\overline{G}]}{1 - \overline{G}_{21} G_{21} K_{22}}, \quad H_{23} = \frac{\overline{G}_{11} G_{21} K_{21}}{1 - \overline{G}_{21} G_{21} K_{22}},$$

$$H_{31} = \frac{K_{12}\overline{G}_{21} G_{22}}{1 - \overline{G}_{21} G_{21} K_{22}}, \quad H_{32} = \frac{K_{12}\overline{G}_{22}}{1 - \overline{G}_{21} G_{21} K_{22}},$$

$$H_{33} = \frac{K_{11} - \overline{G}_{21} G_{21} \det[K]}{1 - \overline{G}_{21} G_{21} K_{22}},$$

where we omit the Laplace index s for simplicity.

The proof of step 2 is similar to that for deriving Eq. (18) in Sec. III. That is, we take the "quantum ideal op-amp assumption" as follows:

$$\frac{\det[G(s)]}{G_{22}(s)} \to 0, \quad \frac{G_{12}(s)}{G_{22}(s)} \to 1, \quad \frac{G_{21}(s)}{G_{22}(s)} \to 1,$$

$$\frac{\det[\overline{G}(s)]}{\overline{G}_{22}(s)} \to 0, \quad \frac{\overline{G}_{12}(s)}{\overline{G}_{22}(s)} \to 1, \quad \frac{\overline{G}_{21}(s)}{\overline{G}_{22}(s)} \to 1,$$

and $G_{11}(s) = G_{22}(s)$ and $\overline{G}_{11}(s) = \overline{G}_{22}(s)$ in the domain $s \in \mathbb{C}$ such that $|G_{11}(s)| \to \infty$ [$\iff |G_{22}(s)| \to \infty$]

and $|\overline{G}_{11}(s)| \to \infty$ [$\iff |\overline{G}_{22}(s)| \to \infty$]. Then in this high-gain limit, the transfer functions are calculated as follows:

$$H_{11} = \frac{G_{12} - \overline{G}_{21} K_{22} \det[G]}{1 - \overline{G}_{21} G_{21} K_{22}},$$

$$= \frac{(G_{12}/G_{22})/\overline{G}_{22} - (\overline{G}_{21}/\overline{G}_{22})K_{22}(\det[G]/G_{22})}{1/(G_{22}\overline{G}_{22}) - (\overline{G}_{21}/\overline{G}_{22})(G_{21}/G_{22})K_{22}},$$

$$\to 0,$$

$$H_{12} = \frac{G_{11}\overline{G}_{22} K_{22}}{1 - \overline{G}_{21} G_{21} K_{22}},$$

$$= \frac{K_{22}}{1/(G_{22}\overline{G}_{22}) - (\overline{G}_{21}/\overline{G}_{22})(G_{21}/G_{22})K_{22}} \to 1,$$

$$H_{13} = \frac{G_{11} K_{21}}{1 - \overline{G}_{21} G_{21} K_{22}},$$

$$= \frac{K_{21}/\overline{G}_{22}}{1/(G_{22}\overline{G}_{22}) - (\overline{G}_{21}/\overline{G}_{22})(G_{21}/G_{22})K_{22}} \to 0,$$

$$H_{21} = \frac{\overline{G}_{11} G_{22}}{1 - \overline{G}_{21} G_{21} K_{22}},$$

$$= \frac{1}{1/(G_{22}\overline{G}_{22}) - (\overline{G}_{21}/\overline{G}_{22})(G_{21}/G_{22})K_{22}} \to -\frac{1}{K_{22}},$$

$$H_{22} = \frac{\overline{G}_{12} + G_{21} K_{22} \det[\overline{G}]}{1 - \overline{G}_{21} G_{21} K_{22}},$$

$$= \frac{(\overline{G}_{12}/\overline{G}_{22})/G_{22} + (G_{21}/G_{22})K_{22}(\det[\overline{G}]/\overline{G}_{22})}{1/(G_{22}\overline{G}_{22}) - (\overline{G}_{21}/\overline{G}_{22})(G_{21}/G_{22})K_{22}},$$

$$\to 0,$$

$$H_{23} = \frac{\overline{G}_{11} G_{21} K_{21}}{1 - \overline{G}_{21} G_{21} K_{22}},$$

$$= \frac{(G_{21}/G_{22})K_{21}}{1/(G_{22}\overline{G}_{22}) - (\overline{G}_{21}/\overline{G}_{22})(G_{21}/G_{22})K_{22}} \to -\frac{K_{21}}{K_{22}},$$

$$H_{31} = \frac{\overline{G}_{21} G_{22} K_{12}}{1 - \overline{G}_{21} G_{21} K_{22}},$$

$$= \frac{(\overline{G}_{21}/\overline{G}_{22})K_{12}}{1/(G_{22}\overline{G}_{22}) - (\overline{G}_{21}/\overline{G}_{22})(G_{21}/G_{22})K_{22}} \to -\frac{K_{12}}{K_{22}},$$

$$H_{32} = \frac{\overline{G}_{22} K_{12}}{1 - \overline{G}_{21} G_{21} K_{22}},$$

$$= \frac{K_{12}/G_{22}}{1/(G_{22}\overline{G}_{22}) - (\overline{G}_{21}/\overline{G}_{22})(G_{21}/G_{22})K_{22}} \to 0,$$

$$H_{33} = \frac{K_{11} - \overline{G}_{21}G_{21}\det[K]}{1 - \overline{G}_{21}G_{21}K_{22}},$$

$$= \frac{K_{11}/(G_{22}\overline{G}_{22}) - (\overline{G}_{21}/\overline{G}_{22})(G_{21}/G_{22})\det[K]}{1/(G_{22}\overline{G}_{22}) - (\overline{G}_{21}/\overline{G}_{22})(G_{21}/G_{22})K_{22}},$$

$$\rightarrow \frac{\det[K]}{K_{22}}.$$

Now we prove Eq. (A3).

Step 3 can be completed by combining Eq. (32), (A1), and (A2). The resulting expressions are found to be

$$G_{11}^{(\mathrm{FB})} = \frac{H_{21} + (H_{11}H_{22} - H_{12}H_{21})K_{22}^*}{1 - H_{12}K_{22}^*}, \tag{A4}$$

$$G_{12}^{(\mathrm{FB})} = \frac{H_{23} + (H_{13}H_{22} - H_{12}H_{23})K_{22}^*}{1 - H_{12}K_{22}^*}, \tag{A5}$$

$$G_{13}^{(\mathrm{FB})} = \frac{H_{22}K_{12}^*}{1 - H_{12}K_{22}^*}, \tag{A6}$$

$$G_{21}^{(\mathrm{FB})} = \frac{H_{31} + (H_{11}H_{32} - H_{12}H_{31})K_{22}^*}{1 - H_{12}K_{22}^*}, \tag{A7}$$

$$G_{22}^{(\mathrm{FB})} = \frac{H_{33} + (H_{13}H_{32} - H_{12}H_{33})K_{22}^*}{1 - H_{12}K_{22}^*}, \tag{A8}$$

$$G_{23}^{(\mathrm{FB})} = \frac{H_{32}K_{12}^*}{1 - H_{12}K_{22}^*}, \tag{A9}$$

$$G_{31}^{(\mathrm{FB})} = \frac{H_{11}K_{21}^*}{1 - H_{12}K_{22}^*}, \tag{A10}$$

$$G_{32}^{(\mathrm{FB})} = \frac{H_{13}K_{21}^*}{1 - H_{12}K_{22}^*}, \tag{A11}$$

$$G_{33}^{(\mathrm{FB})} = \frac{K_{11}^* + H_{12}\left(K_{12}^*K_{21}^* - K_{11}^*K_{22}^*\right)}{1 - H_{12}K_{22}^*}. \tag{A12}$$

Step 4 is done by simply applying Eq. (A3) to the above equations from Eq. (A4) to Eq. (A12), which leads to Eq. (34).

APPENDIX B: THE MATRIX ENTRIES OF A, B_w, C, D

$$A = \begin{bmatrix}
0 & \Omega_M & 0 & 0 & 0 & 0 & 0 & 0 & 0 & 0 & 0 & 0 \\
0 & 0 & \sqrt{2}G_M & 0 & 0 & 0 & 0 & 0 & 0 & 0 & 0 & 0 \\
0 & 0 & -\gamma_{\mathrm{IFO}}/2 & \Delta & 0 & g_{\mathrm{NI}} & 0 & 0 & 0 & 0 & 0 & 0 \\
\sqrt{2}G_M & 0 & -\Delta & -\gamma_{\mathrm{IFO}}/2 & -g_{\mathrm{NI}} & 0 & 0 & 0 & 0 & 0 & 0 & 0 \\
0 & 0 & 0 & g_{\mathrm{NI}} & -\gamma_{1\mathrm{loss}}/2 & 0 & \lambda & 0 & 0 & 0 & 0 & 0 \\
0 & 0 & -g_{\mathrm{NI}} & 0 & 0 & -\gamma_{1\mathrm{loss}}/2 & 0 & -\lambda & 0 & 0 & 0 & 0 \\
0 & 0 & 0 & 0 & \lambda & 0 & 0 & 0 & 0 & 0 & 0 & g_{24} \\
0 & 0 & 0 & 0 & 0 & -\lambda & 0 & 0 & 0 & 0 & -g_{24} & 0 \\
0 & 0 & 0 & 0 & 0 & 0 & 0 & 0 & -\kappa_{3\mathrm{loss}}/2 & 0 & 0 & g_{34} \\
0 & 0 & 0 & 0 & 0 & 0 & 0 & 0 & 0 & -\kappa_{3\mathrm{loss}}/2 & -g_{34} & 0 \\
0 & 0 & 0 & 0 & 0 & 0 & 0 & g_{24} & 0 & g_{34} & -\kappa_{4\mathrm{loss}}/2 & 0 \\
0 & 0 & 0 & 0 & 0 & 0 & -g_{24} & 0 & -g_{34} & 0 & 0 & -\kappa_{4\mathrm{loss}}/2
\end{bmatrix},$$

$$B_w = \begin{bmatrix} 0 & 0 & 0 & 0 & 0 & 0 & 0 & 0 & 0 \\ 1/\sqrt{\hbar M \Omega_M} & 0 & 0 & 0 & 0 & 0 & 0 & 0 & 0 \\ 0 & -\sqrt{\gamma_{\mathrm{IFO}}} & 0 & 0 & 0 & 0 & 0 & 0 & 0 \\ 0 & 0 & -\sqrt{\gamma_{\mathrm{IFO}}} & 0 & 0 & 0 & 0 & 0 & 0 \\ 0 & 0 & 0 & -\sqrt{\gamma_{1\mathrm{loss}}} & 0 & 0 & 0 & 0 & 0 \\ 0 & 0 & 0 & 0 & -\sqrt{\gamma_{1\mathrm{loss}}} & 0 & 0 & 0 & 0 \\ 0 & 0 & 0 & 0 & 0 & 0 & 0 & 0 & 0 \\ 0 & 0 & 0 & 0 & 0 & 0 & 0 & 0 & 0 \\ 0 & 0 & 0 & 0 & 0 & -\sqrt{\kappa_{3\mathrm{loss}}} & 0 & 0 & 0 \\ 0 & 0 & 0 & 0 & 0 & 0 & -\sqrt{\kappa_{3\mathrm{loss}}} & 0 & 0 \\ 0 & 0 & 0 & 0 & 0 & 0 & 0 & -\sqrt{\kappa_{4\mathrm{loss}}} & 0 \\ 0 & 0 & 0 & 0 & 0 & 0 & 0 & 0 & -\sqrt{\kappa_{4\mathrm{loss}}} \end{bmatrix},$$

$$C = \begin{bmatrix} 0 & 0 & \sqrt{\gamma_{\mathrm{IFO}}} & 0 & 0 & 0 & 0 & 0 & 0 & 0 & 0 & 0 \\ 0 & 0 & 0 & \sqrt{\gamma_{\mathrm{IFO}}} & 0 & 0 & 0 & 0 & 0 & 0 & 0 & 0 \end{bmatrix}, \quad D = \begin{bmatrix} 0 & 1 & 0 & 0 & 0 & 0 & 0 & 0 & 0 \\ 0 & 0 & 1 & 0 & 0 & 0 & 0 & 0 & 0 \end{bmatrix},$$

where $G_M = G_{\mathrm{arm}}\sqrt{\hbar/(M\Omega_M)}$.

[1] H. S. Black, Inventing the negative feedback amplifier, IEEE Spectr. **14**, 55 (1977).

[2] H. S. Black, Stabilized feed-back amplifiers, Proc. IEEE **72**, 716 (1984).

[3] Brahim Haraoubia, *Nonlinear Electronics 1* (ISTE Press - Elsevier, London, 2018).

[4] J. M. Courty, F. Grassia, and S. Reynaud, Quantum noise in ideal operational amplifiers, EPL **46**, 31 (1999).

[5] A. A. Clerk, M. H. Devoret, S. M. Girvin, F. Marquardt, and R. J. Schoelkopf, Introduction to quantum noise, measurement, and amplification, Rev. Mod. Phys. **82**, 1155 (2010).

[6] N. Yamamoto, Quantum Feedback Amplification, Phys. Rev. Appl. **5**, 044012 (2016).

[7] H. M. Wiseman and G. J. Milburn, All-optical versus electro-optical quantum-limited feedback, Phys. Rev. A **49**, 4110 (1994).

[8] M. Yanagisawa and H. Kimura, Transfer function approach to quantum control-part I: Dynamics of quantum feedback systems, IEEE Trans. Automat. Control **48**, 2107 (2003).

[9] H. Mabuchi, Coherent-feedback quantum control with a dynamic compensator, Phys. Rev. A **78**, 032323 (2008).

[10] M. R. James, H. I. Nurdin, and I. R. Petersen, H^∞ control of linear quantum stochastic systems, IEEE Trans. Automat. Control **53**, 1787 (2008).

[11] J. Gough and M. R. James, The series product and its application to quantum feedforward and feedback networks, IEEE Trans. Automat. Control **54**, 2530 (2009).

[12] R. Hamerly and H. Mabuchi, Advantages of Coherent Feedback for Cooling Quantum Oscillators, Phys. Rev. Lett. **109**, 173602 (2012).

[13] J. Kerckhoff, R. W. Andrews, H. S. Ku, W. F. Kindel, K. Cicak, R. W. Simmonds, and K. W. Lehnert, Tunable Coupling to a Mechanical Oscillator Circuit Using a Coherent Feedback Network, Phys. Rev. X **3**, 021013 (2013).

[14] N. Yamamoto, Coherent versus Measurement Feedback: Linear Systems Theory for Quantum Information, Phys. Rev. X **4**, 041029 (2014).

[15] H. A. Haus and J. A. Mullen, Quantum noise in linear amplifiers, Phys. Rev. **128**, 2407 (1962).

[16] C. M. Caves, Quantum limits on noise in linear amplifiers, Phys. Rev. D **26**, 1817 (1982).

[17] N. Bergeal, F. Schackert, M. Metcalfe, R. Vijay, V. E. Manucharyan, L. Frunzio, D. E. Prober, R. J. Schoelkopf, S. M. Girvin, and M. H. Devoret, Phase-preserving amplification near the quantum limit with a Josephson ring modulator, Nature **465**, 64 (2010).

[18] C. M. Caves, J. Combes, Z. Jiang, and S. Pandey, Quantum limits on phase-preserving linear amplifiers, Phys. Rev. A **86**, 063802 (2012).

[19] R. Hamerly and H. Mabuchi, Optical Devices Based on Limit Cycles and Amplification in Semiconductor Optical Cavities, Phys. Rev. Appl. **4**, 024016 (2015).

[20] Z. Wang, M. Pechal, E. A. Wollack, P. Arrangoiz-Arriola, M. Gao, N. R. Lee, and A. H. Safavi-Naeini, Quantum Dynamics of a Few-Photon Parametric Oscillator, Phys. Rev. X **9**, 021049 (2019).

[21] W. M. Laghari, M. U. Baloch, M. A. Mengal, and S. J. Shah, Performance analysis of analog Butterworth low pass filter as compared to Chebyshev type-I filter, Chebyshev type-II filter and elliptical filter, Circuits Syst. **5**, 209 (2014).

[22] B. R. Bardhan and J. H. Shapiro, Ultimate capacity of a linear time-invariant bosonic channel, Phys. Rev. A **93**, 032342 (2016).

[23] B. Yurke, Optical back-action-evading amplifiers, J. Opt. Soc. Am. B **2**, 732 (1985).

[24] B. Abdo, K. Sliwa, S. Shankar, M. Hatridge, L. Frunzio, R. Schoelkopf, and M. H. Devoret, Josephson Directional Amplifier for Quantum Measurement of Superconducting Circuits, Phys. Rev. Lett. **112**, 167701 (2014).

[25] A. Metelmann and A. A. Clerk, Nonreciprocal Photon Transmission and Amplification via Reservoir Engineering, Phys. Rev. X **5**, 021025 (2015).

[26] D. Malz, L. D. Tóth, N. R. Bernier, A. K. Feofanov, T. J. Kippenberg, and A. Nunnenkamp, Quantum-Limited Directional Amplifiers with Optomechanics, Phys. Rev. Lett. **120,** 023601 (2018).

[27] B. Abdo, N. T. Bronn, O. Jinka, S. Olivadese, M. Brink, and J. M. Chow, Multi-path interferometric Josephson directional amplifier for qubit readout, Quantum Sci. Technol. **3,** 024003 (2018).

[28] H. Miao, Y. Ma, C. Zhao, and Y. Chen, Enhancing the Bandwidth of Gravitational-Wave Detectors with Unstable Optomechanical Filters, Phys. Rev. Lett. **115,** 211104 (2015).

[29] M. Zhou and S. M. Shahriar, Optomechanical resonator as a negative dispersion medium for enhancing the sensitivity bandwidth in a gravitational-wave detector, Phys. Rev. D **98,** 022003 (2018).

[30] M. Page, J. Qin, J. L. Fontaine, C. Zhao, L. Ju, and D. Blair, Enhanced detection of high frequency gravitational waves using optically diluted optomechanical filters, Phys. Rev. D **97,** 124060 (2018).

[31] J. Bentley, P. Jones, D. Martynov, A. Freise, and H. Miao, Converting the signal-recycling cavity into an unstable optomechanical filter to enhance the detection bandwidth of gravitational-wave detectors, Phys. Rev. D **99,** 102001 (2019).

[32] Z. Y. Ou, S. F. Pereira, and H. J. Kimble, Realization of the Einstein-Podolsky-Rosen paradox for continuous variables in nondegenerate parametric amplification, Appl. Phys. B **55,** 265 (1992).

[33] C. W. Gardiner and P. Zoller, *Quantum Noise* (Springer, Berlin, 2004).

[34] H. I. Nurdin and N. Yamamoto, *Linear Dynamical Quantum Systems* (Springer, New York, 2017).

[35] J. E. Gough, S. Grivopoulos, and I. R. Petersen, Isolated Loops in Quantum Feedback Networks, arXiv:1705.09916 (2017).

[36] K. J. Åström and R. M. Murray, *Feedback Systems* (Princeton University Press, Princeton, 2008).

[37] K. H. Ang, G. Chong, and Y. Li, PID control system analysis, design, and technology, IEEE Trans. Control Syst. Technol. **13,** 559 (2005).

[38] J. E. Gough, A quantum Kalman filter-based PID controller, arXiv:1701.06578 (2017).

[39] H. Chen, H. Li, F. Motzoi, L. Martin, K. B. Whaley, and M. Sarovar, Quantum proportional-integral (PI) control, New J. Phys. **22,** 113014 (2020).

[40] R. L. Hudson and K. R. Parthasarathy, Quantum Ito's formula and stochastic evolutions, Commun. Math. Phys. **93,** 301 (1984).

[41] P. C. Byrne and J. A. Worsham, in *IEEE Proceedings on Southeastcon* (IEEE, New Orleans, 1990), Vol. 1, p. 202.

[42] M. Xu and M. J. Holland, Conditional Ramsey Spectroscopy with Synchronized Atoms, Phys. Rev. Lett. **114,** 103601 (2015).

[43] Y. Kato, N. Yamamoto, and H. Nakao, Semiclassical phase reduction theory for quantum synchronization, Phys. Rev. Res. **1,** 033012 (2019).

[44] A. Kamal, J. Clarke, and M. H. Devoret, Gain, Phys. Rev. B **86,** 144510 (2012).

[45] R. W. Andrews, R. W. Peterson, T. P. Purdy, K. Cicak, R. W. Simmonds, C. A. Regal, and K. W. Lehnert, Bidirectional and efficient conversion between microwave and optical light, Nat. Phys. **10,** 321 (2014).

[46] C. F. Ockeloen-Korppi, E. Damskägg, J.-M. Pirkkalainen, T. T. Heikkilä, F. Massel, and M. A. Sillanpää, Low-Noise Amplification and Frequency Conversion with a Multi-port Microwave Optomechanical Device, Phys. Rev. X **6,** 041024 (2016).

[47] J. Combes, J. Kerckhoff, and M. Sarovar, The SLH framework for modeling quantum input-output networks, Adv. Phys.: X **2,** 784 (2017).

[48] J. Kerckhoff and K. W. Lehnert, Superconducting Microwave Multivibrator Produced by Coherent Feedback, Phys. Rev. Lett. **109,** 153602 (2012).

[49] B. P. Abbott *et al.* (The LIGO Scientific Collaboration and the Virgo Collaboration), Observation of Gravitational Waves from a Binary Black Hole Merger, Phys. Rev. Lett. **116,** 061102 (2016).

[50] G. M. Harry and for the LIGO Scientific Collaboration, Advanced LIGO: The next generation of gravitational wave detectors, Class. Quantum Gravity **27,** 084006 (2010).

[51] F. Acernese *et al.* (The Virgo Collaboration), Quantum Backaction on Kg-Scale Mirrors: Observation of Radiation Pressure Noise in the Advanced Virgo Detector, Phys. Rev. Lett. **125,** 131101 (2020).

[52] K. Somiya and for the KAGRA Collaboration, Detector configuration of KAGRA-the Japanese cryogenic gravitational-wave detector, Class. Quantum Gravity **29,** 124007 (2012).

[53] Y. Ma, Ph. D. thesis, The University of Western Australia, 2015.

[54] S. L. Danilishin and F. Y. Khalili, Quantum measurement theory in gravitational-wave detectors, Living Rev. Relativ. **15,** 5 (2012).

[55] M. Aspelmeyer, T. J. Kippenberg, and F. Marquardt, Cavity optomechanics, Rev. Mod. Phys. **86,** 1391 (2014).

[56] M. H. Wimmer, D. Steinmeyer, K. Hammerer, and M. Heurs, Coherent cancellation of backaction noise in optomechanical force measurements, Phys. Rev. A **89,** 053836 (2014).

[57] H. Miao, Ph. D. thesis, The University of Western Australia, 2010.

[58] Y. Chen, Macroscopic quantum mechanics: Theory and experimental concepts of optomechanics, J. Phys. B **46,** 104001 (2013).

[59] H. Yu *et al.*, Quantum correlations between light and the kilogram-mass mirrors of LIGO, Nature **583,** 43 (2020).

[60] J. Mizuno, K. A. Strain, P. G. Nelson, J. M. Chen, R. Schilling, A. Rüdiger, and W. Winkler and K. Danzmann, Resonant sideband extraction: A new configuration for interferometric gravitational wave detectors, Phys. Lett. A **175,** 273 (1993).

[61] M. Athans, The role and use of the stochastic linear-quadratic-Gaussian problem in control system design, IEEE Trans. Automat. Control **16,** 529 (1971).

[62] M. Poggio, C. L. Degen, H. J. Mamin, and D. Rugar, Feedback Cooling of a Cantilever Fundamental Mode below 5 mK, Phys. Rev. Lett. **99,** 017201 (2007).

[63] A. Buonanno and Y. Chen, Scaling law in signal recycled laser-interferometer gravitational-wave detectors, Phys. Rev. D **67,** 062002 (2003).

[64] O. Crisafulli, N. Tezak, D. B. S. Soh, M. A. Armen, and H. Mabuchi, Squeezed light in an optical parametric oscillator network with coherent feedback quantum control, Opt. Express **21,** 18371 (2013).

[65] S. Iida, M. Yukawa, H. Yonezawa, N. Yamamoto, and A. Furusawa, Experimental demonstration of coherent feedback control on optical field squeezing, IEEE Trans. Automat. Control **57,** 2045 (2012).

[66] M. Silveri, E Zalys-Geller, M. Hatridge, Z. Leghtas, M. H. Devoret, and S. M. Girvin, Theory of remote entanglement via quantum-limited phase-preserving amplification, Phys. Rev. A **93,** 062310 (2016).

[67] N. Bergeal, R. Vijay, V. E. Manucharyan, I. Siddiqi, R. J. Schoelkopf, S. M. Girvin, and M. H. Devoret, Analog information processing at the quantum limit with a Josephson ring modulator, Nat. Phys. **6,** 296 (2010).